Title: TOR coordinates nucleotide availability with ribosome biogenesis in plants

Short Title: TOR coordinates plant nucleotide metabolism

Michael Busche[1,2], M. Regina Scarpin[1,2], Robert Hnasko[3], Jacob O. Brunkard[1,2]*

[1]Department of Plant and Microbial Biology, University of California, Berkeley, CA 94720

[2]Plant Gene Expression Center, USDA Agricultural Research Service, Albany, CA 94710

[3]Produce Safety and Microbiology Research Unit, Western Regional Research Center, Pacific West Area, USDA Agricultural Research Service

*to whom correspondence should be addressed: brunkard@berkeley.edu

The author responsible for distribution of materials integral to the findings presented in this article in accordance with the policy described in the Instructions for Authors (www.plantcell.org) is Jacob O. Brunkard (brunkard@berkeley.edu).

ABSTRACT

TARGET OF RAPAMYCIN (TOR) is a conserved eukaryotic Ser/Thr protein kinase that coordinates growth and metabolism with nutrient availability. We conducted a medium-throughput functional genetic screen to discover essential genes that promote TOR activity in plants, and identified a critical regulatory enzyme, cytosolic phosphoribosyl pyrophosphate (PRPP) synthetase (PRS4). PRS4 synthesizes cytosolic PRPP, a key upstream metabolite in nucleotide synthesis and salvage pathways. We found that *prs4* knockouts are embryo-lethal in *A. thaliana*, and that silencing *PRS4* expression in *N. benthamiana* causes pleiotropic developmental phenotypes, including dwarfism, aberrant leaf shape, and delayed flowering. Transcriptomic analysis revealed that ribosome biogenesis is among the most strongly repressed processes in *prs4* knockdowns. Building on these results, we discovered that TOR activity is inhibited by chemical or genetic disruption of nucleotide biosynthesis, but that this effect can be reversed by supplying plants with physiological levels of nucleotides. Finally, we show that TOR transcriptionally promotes nucleotide biosynthesis to support the demands of ribosomal RNA synthesis. We propose that TOR coordinates ribosome biogenesis with nucleotide availability in plants to maintain metabolic homeostasis and support growth.

Introduction

Phosphorus (P) is an essential element for plant life, but is not highly available in agricultural soils, and is the primary limiting factor for crop yield on more than 30% of global arable land (Vance et al., 2003; López-Arredondo et al., 2014). Crop fertilizers include high levels of phosphate (P_i) to drive plant growth and increase crop yields, but crops only utilize ~20-30% of P_i applied to soils, a significant waste of resources that is also environmentally harmful (López-Arredondo et al., 2014; Correll, 1998). Moreover, P_i mineral deposits are finite, with P_i production from mining predicted to begin declining within fifteen years (Cordell and White, 2011), followed by global depletion of P_i mineral deposits within as little as one century. Current models suggest that P_i fertilizer use will exceed safe planetary boundaries by 2050 without significant technological advances to reduce the need for P_i fertilizers (Springmann et al., 2018). Therefore, a major agronomic goal is to maximize P_i uptake and utilization, including by breeding and gene editing to rewire P_i sensing, signaling, and allocation networks in crop species.

Approximately 50% of the organic phosphorus (P_o) in leaves is incorporated in ribosomal RNA (rRNA) (Veneklaas et al., 2012), with the remaining P_o divided among other RNAs, DNA, phospholipids, and P-esters (phosphorylated metabolites, such as glucose-6-phosphate and free nucleotides, as well as phosphorylated proteins) (Figure 1). Since the majority of P_o is invested in ribosomes, some species in the *Proteaceae* family have adapted to P_i-poor soils by synthesizing relatively few ribosomes, with as little as 40-fold less ribosomes per leaf fresh weight when compared to *Arabidopsis thaliana* (Sulpice et al., 2014). While reducing the number of ribosomes prevents P_i deprivation stress in these plants, the consequential decrease in the rate of protein synthesis dramatically slows plant growth (Sulpice et al., 2014). Balancing the trade-off between P_i demand and growth rates by genetically optimizing ribosome abundance in different tissues and developmental stages in crop species is a promising strategy to reduce agricultural reliance on P_i fertilizers (Veneklaas et al., 2012). Achieving this goal will require deep understanding of the regulation of ribosome biogenesis and the P_i- and P_o-sensing mechanisms in plants.

66 TARGET OF RAPAMYCIN (TOR) is a conserved eukaryotic kinase that broadly
67 coordinates metabolism with nutrient availability (Chantranupong et al., 2015; Shi et al.,
68 2018), and is a crucial regulator of ribosome abundance (Hannan et al., 2003; Delarue
69 et al., 2018). When nutrients are available, TOR is active and promotes anabolism and
70 growth; when nutrients are scarce, TOR is inactive and cells become quiescent, using
71 catabolic pathways for sustenance (Saxton and Sabatini, 2017). Mutations in the TOR
72 signaling network, especially mutations that increase TOR activity, can cause or
73 contribute to a wide range of cancers (Grabiner et al., 2014; Saxton and Sabatini,
74 2017). One consequence of elevated TOR activity in mutated human cell lines is
75 increased ribosome biogenesis, because TOR strongly promotes the expression of
76 ribosomal protein genes, rRNA, and other genes that contribute to ribosome assembly
77 (Pelletier et al., 2017) . As a result, cells with high TOR activity have high nucleotide
78 demands, and are hypersensitive to chemotherapeutic nucleotide biosynthesis inhibitors
79 (Valvezan et al., 2017; Vander Heiden and DeBerardinis, 2017). To meet these
80 nucleotide demands, TOR promotes pyrimidine and purine biosynthesis (Ben-Sahra et
81 al., 2013; Robitaille et al., 2013; Ben-Sahra et al., 2016), effectively reorganizing cellular
82 metabolism to support higher levels of rRNA synthesis. Recent studies have further
83 demonstrated that TOR activity is coordinated with nucleotide availability in human cells
84 (Emmanuel et al., 2017; Hoxhaj et al., 2017). This coordination is proposed to be
85 mediated by GTP levels: under purine-limiting conditions, GTP levels decrease,
86 disabling the small GTPase Rheb that promote TOR activity in humans (Emmanuel et
87 al., 2017; Hoxhaj et al., 2017). Thus, TOR senses nucleotide availability to serve as a
88 metabolic checkpoint that maintains homeostasis by coupling nucleotide demand
89 (primarily rRNA synthesis) with nucleotide biosynthesis.

90 Nucleotide metabolism and signaling are well-studied in humans, because
91 nucleotide homeostasis is often dysregulated in human diseases (Aird and Zhang,
92 2015), but little is known about how plants sense and respond to nucleotides. P_i
93 deprivation can cause a five-fold reduction in free nucleotide levels in plants, making
94 nucleotides a potentially limiting metabolite in soils with poor P_i availability (Theodorou
95 and Plaxton, 1993). In *Chlamydomonas reinhardtii*, a photosynthetic algal species, P_i
96 starvation reduces TOR activity and genetic manipulation of P_i metabolism disrupts TOR

97 signaling, demonstrating that TOR can contribute to the maintenance of P_i homeostasis
98 (Cuoso *et al.*, 2020). A key intermediate in the incorporation of P_i into nucleotides is
99 phosphoribosyl pyrophosphate (PRPP). PRPP is synthesized by phosphoribosyl
100 pyrophosphate synthetase (PRS, sometimes called ribose-phosphate
101 diphosphokinase), which transfers the diphosphoryl group from ATP to ribose-5-
102 phosphate (the end product of the pentose phosphate pathway) in a Mg^{2+}-dependent
103 reaction. PRPP then acts as a donor of phospho-ribose groups for nucleotide and
104 amino acid synthesis, among other biochemical pathways. PRS has emerged as a key
105 regulatory enzyme in human cellular nutrient signaling pathways; for example, PRS-
106 mediated synthesis of PRPP is the rate-limiting step that drives the protein and
107 nucleotide synthesis necessary for tumorigenesis downstream of the Myc oncogene
108 (Cunningham et al., 2014).

109 Plant genomes encode several PRS enzymes, with at least one localized to the
110 plastid and another localized to the cytosol (Figure 1B). Plastids have spatially co-opted
111 many of the PRPP-dependent metabolic pathways in plants, including *de novo* purine,
112 histidine, and tryptophan biosynthesis, the pyrimidine salvage pathway, as well as
113 various metabolic pathways downstream of these molecules, including cytokinin
114 biosynthesis. Cytosolic PRPP is therefore primarily required to regenerate nucleotides
115 via the purine salvage pathway and for *de novo* pyrimidine biosynthesis (Lerbs et al.,
116 1980; Witz et al., 2012). In *Arabidopsis thaliana*, four genes encode organellar PRS
117 enzymes (*PRS1, PRS2, PRS3,* and *PRS5*) and one gene encodes the cytosolic PRS
118 enzyme (*PRS4*) (Ito et al., 2011). Here, we show that *PRS4* is an essential gene in
119 plants that is required to maintain TOR activity. Furthermore, taking a functional
120 genetics approach in *N. benthamiana* and a chemical genetic approach in *A. thaliana*,
121 we specifically demonstrate that nucleotides promote TOR activity, and that TOR
122 transcriptionally promotes nucleotide biosynthesis. We conclude that TOR coordinates
123 nucleotide availability with ribosome biogenesis to maintain P homeostasis in plants.

124

125

126 **Results**

127 ***PRS4* drives TOR activity and plant development**

128 In an effort to identify genes that regulate TOR activity, we conducted a medium-
129 throughput functional genetic screen using virus-induced gene silencing (VIGS) to
130 silence *N. benthamiana* genes that we predicted to be essential for embryogenesis in *A.*
131 *thaliana*. To measure TOR activity after gene silencing, we extracted leaf proteins to
132 prepare Western blots and probed these blots with α-AtS6K-p449, which specifically
133 detects a phosphopeptide on plant S6 KINASE (S6K) that is directly phosphorylated by
134 the TOR kinase complex (Xiong and Sheen, 2012). We found that silencing *PRS4*
135 strongly reduces S6K-pT449 levels compared to mock treatment (Figure 2A). We then
136 probed total S6K protein levels with α-S6K, confirming that total S6K levels do not
137 decrease in TRV::*NbPRS4*, and therefore demonstrating that TOR activity is severely
138 reduced in TRV::*NbPRS4* knockdown leaves (Figure 2A).

139 Knocking down *PRS4* expression with TRV::*NbPRS4* caused a range of dramatic
140 developmental phenotypes (Figure 2B), including delayed flowering, misshapen leaves,
141 dwarfism, and even lethality: 14% of TRV::*NbPRS4* knockdown plants died shortly after
142 *PRS4* silencing was induced (n = 50), whereas none of the mock-treated plants died.
143 Surviving TRV::*NbPRS4* leaves were misshapen and as small as 5% the size of leaves
144 in mock-treated shoots (Figure 2B). Epidermal cells were significantly smaller in
145 TRV::*NbPRS4* plants (71% the size of cells in mock-treated leaves, $n \geq 108$, $p < 10^{-3}$,
146 Figure 2C), but the difference in cell size was not enough to explain the severe
147 reduction in leaf size (Figure 2B), suggesting that *PRS4* is required to promote cell
148 expansion and cell division. In TRV::*NbPRS4* plants, developmental timing of leaf
149 initiation and flowering was severely disrupted. Leaf initiation was delayed or
150 completely arrested three weeks after infiltrating VIGS vectors in TRV::*NbPRS4* plants
151 (Figure 2B). TRV::*NbPRS4* plants flowered two or more weeks later than mock-treated
152 plants, and many TRV::*NbPRS4* knockdowns did not flower at all during our six-week
153 observation period. Despite these clear defects in shoot development, we did not
154 detect any striking morphological phenotype in histological sections of TRV::*NbPRS4*
155 knockdown vegetative shoot apical meristems (Figure 2D). Taken together, these

156 results show that *PRS4* is required for diverse developmental processes, including leaf
157 initiation, expansion, and morphology; the transition from vegetative to reproductive
158 growth; and both cell expansion and cell division.

159 ***PRS4* is essential for plant embryogenesis**

160 As part of a recent high-throughput effort to generate higher order mutations in *A.*
161 *thaliana*, *prs4*/+ was crossed to *prs3/*+, but no offspring in the F_2 generation of this cross
162 were homozygous for *prs4*, hinting that *PRS4* is essential for *A. thaliana* development
163 (Bolle et al., 2013). To test this hypothesis, we obtained a putative T-DNA insertion line
164 in the *PRS4* gene (*At2g42910*), GabiKat-780B11 (Figure 3). Preliminary sequencing
165 suggested that GabiKat-780B11 carries a T-DNA insertion in the third intron of the
166 *PRS4* gene, and is therefore predicted to be a null allele. No other publicly available T-
167 DNA insertion lines are predicted to abolish *PRS4* expression. We confirmed the
168 location of the GabiKat-780B11 T-DNA by PCR (Figure 3A), and named this allele *prs4-*
169 *1*. We isolated several independent *prs4-1*/+ heterozygous plants, allowed the plants to
170 self-fertilize, collected seed, and genotyped the F_1 generation. We identified only *prs4-*
171 *1/*+ heterozygous or +/+ plants in a 2:1 ratio, indicating that *prs4-1/prs4-1* is lethal.

172 To confirm that *prs4-1* is lethal and determine when *prs4-1* mutants arrest, we
173 next examined seeds in the siliques of several *prs4-1*/+ plants from separate families.
174 77% of seeds in these siliques were green with viable embryos, whereas 23% of these
175 seeds were collapsed and brown (Figure 3B). After histochemically clearing the seeds,
176 we observed normal embryo morphology in the green seeds, but could not observe a
177 multicellular embryo in the shrunken seeds (Figure 3C). The green seeds segregated
178 2:1 for *prs4-1/*+ : +/+, as predicted for an embryo-lethal allele. We marked the position
179 of putative *prs4-1/prs4-1* aborted seeds, and noticed that the expected number of seeds
180 near the apex of the silique were aborted (26.7%, n = 180, χ^2 = 0.3, p = 0.61), but less
181 than 20% of seeds near the base of the silique were aborted (18.9%, n = 180, χ^2 = 3.6,
182 p = 0.058), suggesting a slight pollen transmission defect that could explain why only
183 23% of *prs4-1*/+ offspring are homozygous for the null *prs4-1* allele (Meinke, 1985).
184 Finally, we generated stable transgenic lines by transforming *prs4-1*/+ flowers with T-
185 DNAs carrying either $35S_{PRO}$*:PRS4-GFP* or $35S_{PRO}$*:YFP-PRS4* (Figure 3D), both of

186 which rescued the lethal phenotype of *prs4-1/prs4-1* seeds. Therefore, we concluded
187 that *PRS4* is required for the earliest stages of *A. thaliana* sporophyte development.

188 In wild-type *A. thaliana*, *PRS4* transcriptional expression is strongest in
189 metabolically active cells, especially the shoot apical meristem and germinating seeds
190 (Supplemental Figure 1). *PRS4* transcriptional expression is notably lower in quiescent
191 plants, such as seeds entering dormancy and mature pollen grains (Supplemental
192 Figure 1). The expression patterns of genes that encode the organelle-targeted PRS
193 enzymes, *PRS2*, *PRS3*, and *PRS5*, are largely similar to *PRS4*, although *PRS2* is
194 expressed in seeds entering dormancy, and both *PRS2* and *PRS3* are expressed in
195 mature pollen grains (Supplemental Figure 1). *PRS1* is consistently expressed at very
196 low levels during development, in contrast to the other *PRS* genes (Supplemental
197 Figure 1). These expression patterns indicate that PRS enzymes are strongly
198 expressed in both the cytosol and the organelles in all metabolically active
199 developmental stages to support PRPP synthesis.

200 ***PRS4* promotes ribosome biogenesis**

201 To identify disrupted genetic pathways in TRV::*NbPRS4* plants, we took a global
202 transcriptomic approach (Figure 4). Nine RNA-Seq libraries were sequenced from
203 rRNA-depleted RNA extracted from replicated pools of *N. benthamiana* shoot apices
204 (defined as all tissue above the second-youngest leaf, including the shoot meristem,
205 some stem, and the youngest two visible leaves; Supplemental Figure 2). Three
206 libraries each were prepared from mock-silenced plants, TRV::*NbPRS4* plants with
207 "moderate" visible phenotypes (Figure 2B, middle panel), or TRV::*NbPRS4* plants with
208 "severe" visible phenotypes (Figure 2B, bottom panel). RNA-Seq confirmed that *PRS4*
209 expression is effectively silenced in the TRV::*NbPRS4* plants, but not in mock-infected
210 plants, as expected. 35,877 annotated *N. benthamiana* genes were detected in our
211 transcriptomes, of which 4,986 were significantly differentially-expressed genes (DEGs)
212 between TRV::*NbPRS4* and mock-silenced plants (3,213 induced, 1,773 repressed, $p_{adj.}$
213 < 0.05) (Figure 4A, Supplemental Data Sets 1 and 2). This large number of DEGs
214 demonstrates the dramatic effects of disrupting PRS4 activity on cellular homeostasis.
215 We detected relatively few DEGs between TRV::*NbPRS4* plants with "moderate" or

216 “severe” visible phenotypes (489 genes, $p_{adj} < 0.05$) (Figure 4A, Supplemental Data Set
217 3), suggesting that the morphological variation among TRV::*NbPRS4* knockdown plants
218 does not strongly correlate with differences in gene expression. Principal components
219 analysis of the nine transcriptomes also showed that the mock-silenced transcriptomes
220 grouped separately from the TRV::*NbPRS4* knockdown transcriptomes, but that the
221 “moderate” and “severe” groups were not so readily distinguished (Figure 4A).

222 *N. benthamiana* is an emerging model system whose genome has not been
223 extensively annotated, so to develop tools to rigorously analyze the TRV::*NbPRS4*
224 RNA-Seq data, we submitted the entire *N. benthamiana* predicted proteome (genome
225 version 1.0.1) to Mercator4 for functional annotation using the MapMan gene ontology
226 (Lohse et al., 2014). This approach conservatively assigned functions to 23,001
227 annotated genes in *N. benthamiana* (Supplemental Data Set 3), of which 14,502 were
228 detected in our RNA-Seq analysis and 2,662 were DEGs (Supplemental Data Set 1).
229 We then used MapMan to identify enriched functional categories in our transcriptomes,
230 with stringent parameters, using only significant DEGs and the Benjamini-Hochberg-
231 Yekutieli procedure to correct for the false discovery rate. 48 categories were
232 significantly affected in TRV::*NbPRS4* versus mock ($p_{adj} < 0.05$) (Figure 4B,
233 Supplemental Data Set 5), but no categories were significantly affected in the
234 comparison between the visually “severe” and “mild” phenotype pools of TRV::*NbPRS4*
235 plants ($p_{adj} < 0.05$), again supporting the hypothesis that the morphological variation we
236 observed was not due to a consistent difference in the plants’ transcriptional programs.

237 In the TRV::*NbPRS4* transcriptome, one of the most significant effects was
238 downregulation of genes involved in ribosome biogenesis (Figure 4D, Supplemental
239 Data Sets 1, 5). To illustrate, the expression of genes encoding 51 of the 81 plant
240 cytosolic ribosomal proteins were significantly lower in TRV::*NbPRS4* than in mock
241 controls (Figure 4D, Supplemental Data Set 4). TOR has conserved roles in promoting
242 expression of ribosomal protein genes (Cardenas et al., 1999; Hannan et al., 2003;
243 Marion et al., 2004; Xiong et al., 2013a), so their repression likely reflects the
244 suppression of TOR activity in TRV::*NbPRS4* plants. To determine the consequences
245 of ribosome biogenesis transcript downregulation in TRV::*NbPRS4* on overall ribosome

246 abundance, we assayed total rRNA in TRV::*NbPRS4* versus mock plants, and found
247 that rRNA levels were approximately 2-fold lower per fresh weight in TRV::*NbPRS4*
248 knockdown shoots than in mock-treated plants ($n \geq 3$, $p < 0.05$, Figure 4D). Since
249 ribosomes can account for ~60% of nucleotides and ~25% of proteins in a plant cell, a
250 two-fold reduction in ribosome abundance represents a dramatic shift in cellular
251 physiology. Thus, a major effect of knocking down *PRS4* expression is disruption of
252 ribosome biogenesis, likely a consequence of TOR inactivation (Figure 4E).

253 Various other biological processes were also significantly affected in the
254 TRV::*NbPRS4* transcriptomes (Figure 4B). Genes involved in cell cycle progression
255 were broadly repressed, consonant with our observation that both cell size and cell
256 number are significantly lower in TRV::*NbPRS4* leaves. Genes involved in solute
257 transport, nutrient uptake, and stress responses, including genes that encode heat
258 shock proteins and glutathione S-transferases, are among the functional categories that
259 were significantly induced in TRV::*NbPRS4*. The expression of various transcription
260 factor (TF) families were also affected in TRV::*NbPRS4*, with a few strong patterns: TFs
261 typically involved in developmental patterning and differentiation, such as the C2C2 Zn
262 finger, MADS box, GRF, LOB, and homeobox TFs, were generally down-regulated in
263 TRV::*NbPRS4*, whereas TFs typically involved in stress responses, such as ERF, NAC,
264 bZIP, and WRKY TFs, were generally up-regulated in TRV::*NbPRS4* (Figure 4C).
265 Thus, from a global perspective, the TRV::*NbPRS4* transcriptome demonstrates that
266 loss of cytosolic PRPP severely disrupts cellular homeostasis, reprogramming the
267 transcriptome to repress anabolic growth and developmental patterning and to induce a
268 host of stress responses.

269 **Purine and pyrimidine biosynthesis drive TOR activity**

270 PRS4-synthesized cytosolic PRPP contributes primarily to two pathways in
271 plants cells: cytosolic PRPP is condensed with orotate by cytosolic UMP synthase
272 (UMPSase), yielding orotidine 5′-monophosphate (OMP), a precursor in *de novo*
273 pyrimidine biosynthesis; and adenine or hypoxanthine/guanine
274 phosphoribosyltransferases convert adenine and guanine to AMP and GMP,
275 respectively, using cytosolic PRPP in the purine salvage pathway. Since the

276 TRV::*NbPRS4* knockdown drastically reduced TOR activity, we hypothesized that one
277 or both of these pathways—*de novo* pyrimidine synthesis and/or purine salvage—are
278 required to maintain TOR activity in plant cells.

279 To directly test this hypothesis, we expanded our genetic screen to silence genes
280 that encode nucleotide biosynthesis enzymes in *N. benthamiana*. Specifically, we
281 designed VIGS triggers to target critical genes in the *de novo* purine biosynthesis
282 pathway (*PHOSPHORIBOSYLGLYCINAMIDE FORMYLTRANSFERASE*, or *GART*;
283 *ADENYLOSUCCINATE LYASE*, or *ASL*; and *PHOSPHORIBOSYLAMINOIMIDAZOLE*
284 *CARBOXAMIDE FORMYLTRASFERASE / INOSINE MONOSPHOSPHATE*
285 *CYCLOHYDROLASE*, or *ATIC*) or in the *de novo* pyrimidine biosynthesis pathway
286 (*DIHYDROOROTASE*, or *DHOase*; *DIHYDROOROTATE DEHYDROGENASE*, or
287 *DHODH*; and *URIDINE MONOPHOSPHATE SYNTHASE*, or *UMPSase*). We selected
288 these enzymes because they do not directly consume ATP or amino acids, and thus are
289 specifically disrupting only nucleotide biosynthesis (and not incidentally impacting other
290 primary metabolic pathways). Across experiments, silencing expression of enzymes in
291 *de novo* pyrimidine or purine biosynthesis disrupted plant development and physiology,
292 causing delayed growth, reduced leaf size, and striking chlorosis, among other
293 phenotypes (Figure 5A). Strikingly, TOR activity was severely reduced after silencing
294 genes involved in either *de novo* purine or pyrimidine biosynthesis, confirming our
295 hypothesis that nucleotide biosynthesis is required to maintain TOR activity in plants
296 (Figure 5B).

297 **Chemically inhibiting nucleotide biosynthesis inactivates TOR**

298 We next tested whether the hypothesis that nucleotide biosynthesis drives TOR
299 activity is conserved across plant species by investigating the effects of inhibiting
300 nucleotide biosynthesis in *A. thaliana*. For this chemical genetic approach, we treated
301 *A. thaliana* seedlings with inhibitors that specifically impact one or both of the PRS4-
302 dependent nucleotide biosynthesis pathways, and then assayed for changes in TOR
303 activity indicated by altered phosphorylation of S6K-T449. We screened four
304 compounds that target processes that require cytosolic PRPP (Figure 6A). 5-
305 fluorouracil (5FU) and 5-fluoroorotic acid (5FOA) limit only *de novo* pyrimidine synthesis

306 by inhibiting UMPSase and thymidylate synthetase activity, respectively (Figure 6A). 6-
307 mercaptopurine (6MP) specifically limits the purine salvage pathway by inhibiting PRPP
308 transfer to purines by hypoxanthine phosphoribosyltransferases (Figure 6A).
309 Methotrexate (MTX) limits both purine and pyrimidine biosynthesis by inhibiting
310 dihydrofolate reductase, which is required for folate synthesis, a necessary nucleotide
311 precursor (Figure 6A). To assay the effects of these inhibitors, seedlings were grown in
312 ½ MS media for three days, then transferred to fresh ½ MS media supplemented with
313 15 mM glucose and 10 μM of one of the nucleotide biosynthesis inhibitors, or a mock
314 treatment as a negative control. Seedlings were collected 24 h after treatment and
315 proteins were extracted and analyzed by Western blot (Figure 6C). Under these
316 conditions, MTX had the strongest effects. *De novo* pyrimidine synthesis inhibitors 5FU
317 and 5FOA had less potent effects. 6MP, an inhibitor of the purine salvage pathway, had
318 no noticeable effect on TOR activity, as reflected by S6K-pT449 levels. Some seedlings
319 were left in media for 7 days after treatment to observe the inhibitors' long-term effects
320 on growth (Figure 6B). As in the western blot, MTX had the most severe effect on shoot
321 and root growth (Figure 6B).

322 To demonstrate specificity and further investigate the effects of the nucleotide
323 biosynthesis inhibitors that were most effective at reducing TOR activity (Figure 6C), we
324 performed this assay again with a range of concentrations (0.1 μM, 1.0 μM, 5.0 μM, 10
325 μM, or 20 μM) of MTX and 5FOA. Consistent with our previous result, we found that
326 MTX had the strongest effect, partially inhibiting growth and lowering S6K-pT449 levels
327 even at a very low concentration of 0.1 μM. Treatment with 5.0 μM or more MTX
328 caused nearly complete growth arrest, chlorosis, and an even greater decrease in S6K-
329 pTT49 levels (Figure 6D and 6E). Low concentrations of 5FOA slightly reduced growth
330 and had some impact on S6K-pT449 levels, whereas higher concentrations (5.0 μM to
331 20 μM) strongly inhibited growth and reduced S6K-pT449 levels (Figure 6F and 6G).
332 Thus, we concluded that complete inhibition of *de novo* nucleotide synthesis by MTX
333 was most effective at inhibiting TOR, inhibition of *de novo* pyrimidine synthesis was
334 sufficient to lower TOR activity, and the purine salvage pathway was not needed to
335 maintain TOR activity under these growth conditions. Given the potent impact of MTX
336 on TOR activity, we focused further experiments on MTX treatments.

337 **Resupplying nucleotides restores TOR activity**

338 First, we conducted a time course to determine how quickly MTX treatment
339 impacts TOR activity. For these experiments, we used 0.1 μM MTX, which was an
340 approximately minimal concentration to inhibit TOR activity 24 h after treatment. 2 h
341 after MTX treatment, S6K-pT449 levels were not yet lower (Figure 7A). S6K-pT449
342 levels rapidly decreased over the next four hours, while total S6K levels remained stable
343 (Figure 7A). Therefore, under our experimental conditions, MTX begins to lower TOR
344 activity 3 to 4 h after treatment, ultimately abolishing S6K-pT449 levels by 24 h after
345 treatment. This is consonant with past experiments using comparable experimental
346 conditions, which showed that MTX requires at least ~2-6 hours to begin to affect plant
347 metabolism (Loizeau et al., 2008). To test the hypothesis that MTX inhibition of TOR
348 activity is due to nucleotide depletion, we supplemented MTX-treated seedlings with 0.5
349 mM, 1.0 mM or 2.0 mM nucleotides: inosine monophosphates (IMPs), uracil
350 monophosphates (UMPs), or a mixture of all nucleotide monophosphates (NMPs). We
351 chose these concentrations because 1.0 – 2.0 mM nucleotides are a physiologically-
352 relevant concentration (Chen et al., 2000). Neither IMPs nor UMPs were able to restore
353 TOR activity after 3.5 h, in agreement with our results above suggesting that both purine
354 and pyrimidine synthesis are required to maintain TOR activity in plants (Figure 7B and
355 C). A mixture of all NMPs, however, was sufficient to significantly increase S6K-pT449
356 levels 3.5 h after treatment (Figure 7D). In summary, these experiments demonstrate
357 that nucleotides are sufficient to activate TOR in MTX-treated seedlings. Therefore, we
358 concluded that MTX inhibits TOR specifically by limiting nucleotide biosynthesis.
359 Moreover, in agreement with our hypothesis that TRV::*NbPRS4* knockdowns reduce
360 TOR activity due to limited nucleotide biosynthesis, these results directly demonstrate
361 that TOR is sensitive to nucleotide availability in plants.

362 **TOR promotes expression of *de novo* nucleotide biosynthesis genes**

363 Among its many metabolic roles, TOR is known to promote nucleotide
364 biosynthesis in animals and fungi through transcriptional and post-translational control
365 (Ben-Sahra et al., 2013; Robitaille et al., 2013; Ben-Sahra et al., 2016). We therefore
366 hypothesized that TOR could also transcriptionally promote nucleotide biosynthesis in

367 plants. To test this hypothesis, we mined publicly available transcriptomic datasets,
368 focusing on changes in expression of genes that encode nucleotide metabolic enzymes.
369 We found that genes involved in nucleotide biosynthesis are enriched among the genes
370 upregulated by the glucose-TOR transcriptional program ($p < 0.01$), as previously noted
371 (Xiong et al., 2013a), and among the genes repressed when plants are treated with the
372 TOR inhibitor AZD-8055 ($p < 0.05$) (Dong et al., 2015). Indeed, transcripts encoding
373 enzymes of nearly every step of purine biosynthesis downstream from PRS-mediated
374 PRPP synthesis are induced when TOR is activated and repressed when TOR is
375 inactivated (Figure 8A). Several pyrimidine biosynthesis enzyme genes are also
376 transcriptionally induced by TOR activation and transcriptionally repressed by TOR
377 inactivation (Figure 8A). Moreover, genes encoding purine and pyrimidine salvage
378 pathway enzymes and genes that promote DNA synthesis are also transcriptionally
379 promoted by TOR (Supplemental Data Set 6). Alongside promoting nucleotide
380 biosynthesis, TOR transcriptionally controls nucleotide catabolism: genes involved in P_i
381 salvage, nucleotide degradation, and purine importers are all induced when TOR is
382 inactivated, whereas genes involved in P_i salvage are repressed when TOR is
383 activated. For instance, several NUDIX hydrolases (*NUDT8*, *NUDT13*, and *NUDT15*)
384 are repressed ~2-3.5-fold when TOR is activated by glucose (Supplemental Data Set 6).
385 In concert, these data demonstrate that TOR activation broadly reprograms the plant
386 transcriptome to promote nucleotide biosynthesis and repress nucleotide catabolism.

387 We next reanalyzed the transcriptome of MTX-treated *A. thaliana* cells (Loizeau
388 et al., 2008) to test how nucleotide deprivation impacts the *A. thaliana* transcriptional
389 program. Using stringent cutoffs, our analysis revealed 16, 1,748, and 2,485 genes that
390 are differentially expressed 2 h, 6 h, and 24 h after treatment with MTX, respectively,
391 compared to mock-treated cells (Supplemental Data Set 6). The remarkably low
392 number of DEGs detected 2 h after MTX treatment is in keeping with our conclusion
393 above that MTX treatment has effectively no impact on TOR activity 2 h after treatment.
394 Therefore, we focused our analysis on the other two timepoints, 6 h and 24 h after MTX
395 treatment. The biological functions of the DEGs 6 h and 24 h after MTX treatment are
396 largely similar. Broadly, MTX treatment represses expression of genes involved in
397 ribosome biogenesis, mitochondrial oxidative phosphorylation (OXHPOS), and

398 photosynthesis, while inducing expression of E3 ubiquitin ligases that promote protein
399 degradation and amino acid recycling, WRKY and AP2/EREBP transcription factors
400 involved in stress responses, and various starvation response genes, e.g., the *DARK-*
401 *INDUCIBLE* (*DIN*) genes *DIN2*, *DIN6*, and *DIN10* (Supplemental Data Sets 6 and 7).
402 As with the TRV::*NbPRS4* transcriptome, many of these gene categories are conserved
403 targets of TOR, such as ribosomal protein genes and mitochondrial OXPHOS
404 components, which are consistently induced by TOR activity throughout eukaryotic
405 lineages. Indeed, we found that the set of genes regulated by 24 h treatment with AZD-
406 8055, a highly specific ATP-competitive TOR kinase inhibitor, significantly overlapped
407 with the set of genes regulated by 24 h treatment with MTX (553 genes, $p < 10^{-69}$; for
408 comparison, the maximum expected overlapping genes is 292, $p = 0.05$), and that these
409 overlapping genes are almost all co-regulated (503 genes, or 91%, are either induced or
410 repressed in both MTX- and AZD-8055 transcriptomes) (Figure 8C, Supplemental Data
411 Set 6). The striking similarity between the transcriptional profiles of MTX- and AZD-
412 8055-treated *A. thaliana* demonstrates that many of the effects of MTX-mediated
413 nucleotide depletion can be reproduced by TOR inhibition, indicating that nucleotide
414 sensing by TOR is a crucial signaling axis to maintain metabolic homeostasis (Figure
415 8D).

416

417 **Discussion**

418 **Functional genetics to probe TOR signaling networks**

419 TOR is an essential regulatory kinase across all lineages of eukaryotes
420 (Chantranupong et al., 2015). In *A. thaliana*, null *tor* alleles cause embryo arrest at
421 early stages of embryogenesis (Menand et al., 2002). Chemically inhibiting TOR kinase
422 activity or genetically silencing *TOR* expression causes plant growth arrest at later
423 stages of development (Ahn et al., 2011; Montané and Menand, 2013; Xiong et al.,
424 2013b). Therefore, we hypothesized that loss of genes required for activity would likely
425 also be embryo-lethal. To circumvent conducting an arduous forward genetic screen of
426 embryo-lethal mutants (Kim et al., 2002), we took a "fast reverse genetics" approach
427 (Baulcombe, 1999), silencing predicted embryo-lethal genes in *N. benthamiana* during
428 vegetative development with virus-induced gene silencing. With this approach, we
429 discovered that plant TOR activity is sensitive to nucleotide availability in plants,
430 consonant with the recent discovery that mammalian TOR also senses nucleotide
431 availability (Hoxhaj et al., 2017; Emmanuel et al., 2017).

432 Silencing embryo-lethal genes with VIGS does not always cause severe
433 developmental phenotypes (Stonebloom et al., 2009; Burch-Smith and Zambryski,
434 2010; Burch-Smith et al., 2011), but silencing the cytosolic phosphoribosyl
435 pyrophosphate synthetase, *PRS4*, dramatically disrupted plant growth and
436 development. It should be noted that TRV::*NbPRS4* knockdown phenotypes are more
437 severe than TRV::*NbTOR* knockdown phenotypes (Ahn et al., 2011), suggesting that
438 loss of cytosolic PRPP does not exclusively arrest growth via inhibition of the TOR
439 signaling pathway. Similarly, homozygous *prs4-1* knockout embryos arrest at the very
440 earliest stages of embryogenesis, whereas homozygous *tor* knockout embryos arrest at
441 the globular stage. We speculate that the more severe phenotypes of TRV::*NbPRS4*
442 knockdowns and knockouts reflect its absolute requirement for nucleotide biosynthesis
443 to support DNA synthesis during cell division.

444 **TOR coordinates nucleotide metabolism with ribosome biogenesis**

445 In plant leaves, 40-60% of P_o is incorporated in ribosomal RNA (rRNA). rRNA
446 expression and stability are directly controlled by TOR, which promotes expression of
447 ribosomal protein genes, rRNA, and other genes involved in ribosome biogenesis (Ren
448 et al., 2011; Kim et al., 2014). In mutant human cell lines with high TOR activity,
449 overproduction of rRNA disrupts nucleotide homeostasis, making nucleotides less
450 available for other biological processes (Valvezan et al., 2017). As a consequence,
451 these cell lines are hypersensitive to nucleotide synthesis inhibitors, which rapidly
452 deplete nucleotide availability for DNA replication, ultimately triggering DNA damage
453 responses and cell death (Valvezan et al., 2017). Here, we have shown that TOR
454 similarly coordinates nucleotide supply and demand in plant cells. TOR promotes
455 transcription of genes involved in nucleotide biosynthesis and ribosome biogenesis. If
456 nucleotide levels decrease due to another nutritional limitation or physiological stress,
457 i.e., despite the transcriptional promotion of nucleotide biosynthesis by TOR, TOR
458 activity decreases, reducing the demand for nucleotides by ribosome biogenesis.
459 Based on our findings, and by analogy to the human nucleotide-TOR signaling pathway
460 (Valvezan and Manning, 2019), we propose that TOR acts as a molecular rheostat to
461 maintain nucleotide homeostasis in plant cells (Figure 6D).

462 The mechanism of nucleotide sensing by TOR in plants remains unresolved by
463 this study. In human cells, nucleotide depletion is currently proposed to act through the
464 TSC-Rheb signaling axis to inhibit TOR activity (Emmanuel et al., 2017; Hoxhaj et al.,
465 2017). Rheb is a small GTPase that activates TOR at the lysosomal surface, and Rheb
466 engages TOR when growth factor signals suppress its GTPase-activating protein
467 complex, TSC. In nucleotide-depleted cells, Rheb GTP-loading decreases, and its
468 localization, stability, and activity are compromised (Emmanuel et al., 2017; Hoxhaj et
469 al., 2017). Neither Rheb nor TSC are deeply conserved in eukaryotic lineages, so
470 plants must have evolved a distinct mechanism for sensing nucleotide availability.
471 Identifying the nucleotide sensor will be aided by ongoing efforts to elucidate the plant
472 TOR signaling network (Wu et al., 2019).

473 **TOR and P_o sensing for sustainable agriculture**

474 The TOR signaling network is a promising candidate for improving agricultural
475 crops. Current agricultural systems are unsustainable, but biotechnological
476 enhancement of crops can make significant contributions to sustainability efforts
477 (Springmann et al., 2018). To date, most studies of nutrient sensing in plants have
478 focused on pathways that detect inorganic nutrients, such as nitrate, ammonium, and
479 phosphate (Chiou and Lin, 2011; Xu et al., 2012). In natural settings, however, plants
480 consume both inorganic and organic nutrients, such as dissolved P_o and amino acids
481 (Näsholm et al., 1998). Moreover, once nutrients are absorbed by plants, many species
482 rapidly convert inorganic nitrogen and phosphate to organic forms for transport and
483 metabolism. Therefore, understanding the mechanisms of organic nutrient sensing in
484 plants, including the TOR signaling network, should accelerate efforts to develop
485 sustainable agricultural crop varieties.

486 Here, we showed that TOR is sensitive to nucleotide availability, a major fraction
487 of the P_o available for anabolism (Figure 1A, 8D). Moreover, TOR activity strongly
488 promotes synthesis of nucleotides and ribosomal nucleic acids to support the high
489 ribosome abundance required for protein translation in metabolically-active cells.
490 Accordingly, genetically or chemically dampening TOR activity could reduce
491 phosphorus demands, by drastically decreasing the rate of nucleotide and nucleic acid
492 synthesis. Alternatively, for plants grown with excess phosphorus supply, stimulating
493 TOR activity could increase growth rates and crop yields by increasing phosphorus use
494 efficiency and allocation of phosphorus to bioactive, productive macromolecules
495 (nucleotides and rRNA). Therefore, rewiring the TOR signaling network in crop species
496 could theoretically contribute to enhancing crop yields and reducing reliance on
497 fertilizers.

498

499 **Methods**

500 **Plant materials and growth conditions**

501 Plants were grown under standard conditions with 16 h day / 8 h night at ~120
502 µmol photons m^{-2} s^{-1} of photosynthetically active radiation and at 22°C-24°C unless
503 otherwise stated. The inbred Col-0 ecotype was used as wild-type for all *A. thaliana*
504 seedling experiments. GabiKat-780B11, which had been previously described (Bolle et
505 al., 2013), was obtained from the Arabidopsis Biological Resources Center. The
506 reference inbred Nb-1 ecotype, obtained from the Boyce Thompson Institute, was used
507 for all *N. benthamiana* experiments. *prs4-1* was genotyped by extracting DNA from Col-
508 0 plants by grinding snap-frozen leaf tissue in DNA extraction buffer (200 mM Tris-Cl at
509 pH 5.7, 250 mM NaCl, 25 mM EDTA, 0.5% SDS), precipitating DNA in isopropanol,
510 washing DNA with 70% ethanol, and resuspending purified DNA in ddH_2O. PCRs were
511 used to assay for wild-type or T-DNA insertion alleles in 20 µL reactions using GoTaq
512 Green Master Mix (Promega) using manufacturer's instructions and 30 cycles as
513 follows: 95°C for 30 seconds, 57°C for 30 seconds, and 72°C for 60 seconds.
514 Genotyping primers used were: 5′-CAA GGA TTG TCT CTA ATA TCC CCA-3′ (left
515 genomic primer, LP), 5′-CTT TGG GAA GAC ACC ATG AGT TAC-3′ (right genomic
516 primer, RP), and 5′-ATA ATA ACG CTG CGG ACA TCT ACA TTT T-3′ (T-DNA border
517 primer, LB).

518 **Molecular cloning**

519 Virus-induced gene silencing vectors were prepared as previously described
520 (Brunkard et al., 2015). Briefly, RNA was isolated from Nb-1 shoots with the Spectrum
521 Plant Total RNA kit (Sigma-Aldrich) with on-column DNase I digestion (New England
522 Biolabs). cDNA was synthesized from RNA using random hexamers and SuperScript III
523 reverse transcriptase (Fisher Scientific). The *NbPRS4* silencing trigger was amplified
524 with Phusion DNA polymerase (New England Biolabs) using oligonucleotides 5′-GCA
525 TCT AGA ATG GAG AAT GGT GCG C-3′ and 5′-GAT CTC GAG TTC AAC AGT GGG
526 ATA CC-3′ as primers. The amplified *NbPRS4* PCR product was gel purified (Monarch
527 DNA Gel Extraction Kit, New England Biolabs), digested with XbaI and XhoI (New
528 England Biolabs), and ligated with XbaI- and XhoI-digested pYL156 (Liu et al., 2002)

529 using T4 DNA ligase (Promega). Ligations were transformed into house-made
530 chemically competent *E .coli* DH10B. The silencing triggers for all other nucleotide
531 biosynthesis genes were amplified with Phusion DNA polymerase (New England
532 Biolabs) using the oligonucleotides listed in Supplemental Data Set 8. The amplified
533 products were gel purified (Monarch DNA Gel Extraction Kit, New England Biolabs) and
534 incubated with 100 ng XbaI- and XhoI-digested pYL156 in a molar ratio of 1 vector : 2
535 insert. Reactions were incubated with T4 DNA polymerase (New England Biolabs) in
536 NEBuffer 2.1 (New England Biolabs) for 2.5 minutes at room temperature, placed on ice
537 for 10 minutes, and then transformed into house-made chemically competent *E .coli*
538 DH10B. Plasmids were then miniprepped with Bioneer kits, Sanger sequenced to
539 confirm insert sequences, and transformed into *Agrobacterium* GV3101.
540 Manufacturer's protocols were followed throughout.

541 To clone *AtPRS4* for complementation experiments, cDNA was synthesized from
542 RNA isolated from Col-0 rosette leaves, using the techniques described above. *PRS4*
543 was amplified by PCR using oligonucleotides 5′-cacc ATG TCT GAG AAC GCA GCC A-
544 3′ and 5′-AAT CTG CAG AGC ATC AGC AAT-3′ and ligated with topoisomerase into a
545 Gateway entry vector (pENTR/D-TOPO, ThermoFisher). This vector was then digested
546 with EcoRV (New England Biolabs) and recombined with pEarleyGate expression
547 vectors pEarleyGate103 and pEarleyGate104 (Earley et al., 2006) using LR Clonase II
548 (ThermoFisher). After the sequence of these vectors was confirmed, each was
549 transformed into *Agrobacterium* GV3101 for subsequent transformation of plants.

550 **TOR activity assays**

551 *A. thaliana* seedlings or *N. benthamiana* leaves were snap-frozen in liquid
552 nitrogen. Protein was then extracted from the plant tissue in 100 mM MOPS (pH 7.6),
553 100 mM NaCl, 5% SDS, 0.5% β-mercaptoethanol, 10% glycerin, 2 mM PMSF, and 1x
554 PhosSTOP phosphatase inhibitor (Sigma-Aldrich). S6K-pT449 was detected by
555 Western blot using a phosphospecific antibody (ab207399, AbCam) and an HRP-
556 conjugated goat anti-rabbit IgG secondary antibody (Jackson Immuno Research, no.
557 111-035-003). S6K levels were detected by Western blot using a custom monoclonal
558 antibody described below. Total protein was visualized after transfer using Ponceau S

559 red staining. Western blot images were scanned, converted to grayscale, and adjusted
560 for contrast and brightness using ImageJ.

561 To generate monoclonal antibodies that detect total S6K protein levels, peptides
562 were synthesized that corresponded to amino acids 439 through 459 surrounding the
563 TOR substrate T449 in AtS6K1 (At3g08730.1) with either threonine or
564 phosphothreonine at T449 (DPKANPFTNFTYVRPPPSFLH or
565 DPKANPFTNFpTYVRPPPSFLH) and conjugated to either BSA or KLH (GenScript).
566 BSA-conjugated phosphopeptide was used to immunize mice. Sera were screened
567 with enzyme-linked immunosorbet assays (ELISAs) for reactivity to KLH-conjugated
568 peptide and/or phosphopeptide. Subsequent screening of hybridomas with ELISAs
569 using KLH-conjugated peptide or phosphopeptide and Western blots against S6K
570 protein identified a monoclonal antibody that reliably detects total S6K protein levels,
571 regardless of phosphorylation status of T449. Throughout, we refer to this monoclonal
572 antibody as αS6K. In one preliminary experiment (Fig. 6C), we used a commercially-
573 available polyclonal antibody that detects total S6K levels (sc-230, Santa Cruz
574 Biotechnology); we refer to this antibody as pAb-αS6K.

575 **Virus-induced gene silencing**

576 VIGS was performed as previously described (Brunkard et al., 2015). Briefly,
577 *Agrobacterium* cultures carrying either pYL156 containing the silencing trigger or
578 pYL192 were grown overnight in LB with antibiotics at 28°C. Cultures were spun down
579 at 700 x *g* for 10 minutes, washed, and resuspended to OD_{600nm} = 1.0 in 10 mM $MgCl_2$,
580 10 mM 2-(*N*-morpholino)ethanesulfonic (MES) acid (pH = 5.7, adjusted with KOH), and
581 200 μM acetosyringone from a recently-prepared 100mM stock solution frozen in
582 DMSO. Agrobacteria were left to induce virulence at room temperature for 2-4 h with
583 gentle shaking before pressure infiltration into 3-week old *N. benthamiana* leaves by
584 needleless syringe. Plants were returned to standard growth conditions and monitored.
585 Tissue collection and phenotypic observation were performed 2 weeks post-infiltration.
586 TRV::*NbPDS* was used as a positive control to track viral infection and VIGS efficiency,
587 and TRV::*GUS* (pYC1) was used as a mock treatment negative control (Stonebloom et

588 al., 2009). Each gene was silenced in at least 6 plants per experiment. All VIGS
589 experiments were performed at least 3 times.

590 **Phenotypic analysis of TRV::*NbPRS4* plants**

591 All phenotypic analyses and photography of TRV::*NbPRS4* plants were
592 performed 2 weeks post-agroinfiltration. Shoot apices were collected for histology and
593 SEM analysis. The 4th youngest leaf (i.e., the 4th leaf counting down from the apex of
594 each plant) was used for quantifying epidermal cell size. Forceps were used to peel off
595 sections of epidermis from the adaxial side of the leaf, which was then observed under
596 a compound light microscope with a 40x objective. Cells were outlined manually in
597 ImageJ to determine area in square micrometers. Measurements were performed on
598 GUS ("mock") and "moderate" TRV::*NbPRS4* individuals, as tissue from "severe" plants
599 was too fragile to process. Plants unused in other experiments were allowed to grow
600 indefinitely so leaf initiation rate, leaf morphology, and flowering time could be observed.
601 To quantify rRNA levels, total RNA was extracted using the Sigma Spectrum™ Plant
602 Total RNA kit and analyzed using the Agilent RNA 6000 Pico Chip with the Agilent
603 Bioanalyzer 2100.

604 For histology, meristems were harvested from *N. benthamiana* two weeks after
605 inoculation with *Agrobacterium* cultures carrying either pYL156::NbPRS4 or
606 pYL156::GUS (pYC1). Meristems were vacuum infiltrated with infiltration solution (50%
607 ethanol, 5.0% acetic acid, 3.7% formaldehyde) at 15 Hg for 15 minutes. Tissue was
608 dehydrated through a stepwise ethanol dehydration series (15%, 20%, 50%, 75%, 95%)
609 with 15-minute incubations at each step and stored overnight in 95% ethanol + 0.1%
610 Eosin solution. Samples were washed for 20 minutes with the following solutions: 100%
611 ethanol (twice), 75% ethanol + 25% Histoclear, 50% ethanol + 50% Histoclear, 25%
612 ethanol + 75% Histoclear, 100% Histoclear (twice). Tissue was stored overnight in 1:1
613 Histoclear : melted paraplast solution. The next morning, Histoclear : paraplast solution
614 was removed and replaced with melted paraplast. Samples were incubated at 56°C for
615 8-10 hours. Paraplast was replaced every 8-10 hours six additional times. Samples
616 were poured into plastic weighboats, allowed to harden, sectioned, and mounted onto
617 slides. Slides were rehydrated through an ethanol series (100%, 100%, 95%, 85%,

618 70%, 50%, 30%, 15%), stained in 0.1% toluidine blue, and then partially dehydrated
619 through an ethanol series (15%, 30%, 50%, 70%) to destain slightly. Slides were
620 hydrated again (70%, 50%, 30%, 15%) and rinsed in distilled water. Mounted tissue was
621 treated with ImmunoHistoMount and covered with a cover slip. Meristems were
622 visualized with a compound microscope.

623 **Phenotypic analysis of *prs4-1* mutants**

624 *prs4-1 /* + heterozygous *A. thaliana* mutants were allowed to self-fertilize for
625 analysis of homozygous *prs4-1 / prs4-1* progeny in siliques. The location of
626 homozygous *prs4-1* / *prs4-1* progeny along siliques was marked following standard
627 protocols (seedgenes.org). For positional analysis, the number of aborted seeds in the
628 first ten seeds from the silique base (i.e., seeds #1 through #10) and in the second ten
629 seeds from the silique base (i.e., seeds #11 through #20) was counted in nine
630 independent siliques at comparable developmental stages from several independent
631 *prs4-1* / + parents. Seed abortion was not observed in these positions in wild-type
632 siblings grown under the same conditions. Chi-square tests were used to compare the
633 frequency of aborted seeds in these positions to the expected frequency (25%) of
634 aborted seeds. To visualize embryos in *prs4-1* / + progeny, *A. thaliana* seeds were
635 removed from young siliques and placed on one drop of Hoyer's solution on a
636 microscope side. Embryos were visualized with a compound microscope after one hour
637 of clearing in Hoyer's solution.

638 **RNA-Seq and transcriptome analysis**

639 Tissue for RNA-Seq was collected from TRV::*NbPRS4* or mock-treated plants 2
640 weeks post-agroinfiltration with TRV binary vectors. Plant apices, including the youngest
641 2-3 leaves, were collected and immediately frozen in liquid nitrogen. 9 mock-treated
642 individuals, 9 TRV::*NbPRS4* individuals that showed "severe" phenotypic abnormalities,
643 and 9 "moderate" TRV::*NbPRS4* individuals were collected. RNA was extracted using
644 Sigma Spectrum™ Plant Total RNA kit. 3 pools of RNA from 3 individuals were
645 prepared for the mock, severe, and moderate collections. RNA pools were made by
646 combining 333.3 ng of RNA from each individual. Illumina TruSeq Stranded Total RNA
647 kit with Ribo-Zero Plant was used to prepare libraries for RNA sequencing. Libraries

648 were sequenced at the Vincent J. Coates Genomics Laboratory (QB3) using the
649 Illumina Hi-Seq 4000. Reads were aligned with HISAT2 (Kim et al., 2015) and counted
650 with HTSeq (Anders et al., 2015). Differential transcript abundance was determined
651 with DESeq2 (Love et al., 2014).

652 The methotrexate-treated transcriptome was previously described (Loizeau et al.,
653 2008); briefly, cells were treated with 100 μM methotrexate or mock-treated for 2 h, 6 h,
654 or 24 h, RNA was extracted, and cRNA was hybridized with the CATMA array to detect
655 changes in transcript levels. Only transcripts that were detected at significantly different
656 levels in both treatment replicates ($p < 0.05$) were considered significant DEGs here.

657 *PRS* expression profiles during plant development were obtained from the Bio-
658 Analytic Resource for Plant Biology (bar.utoronto.ca) with expression data and an
659 electronic Fluorescent Pictograph (eFP) developed for AtGenExpress (Schmid et al.,
660 2005).

661 Transcriptomes were further analyzed with MapMan software (Thimm et al.,
662 2004). The *N. benthamiana* genome was annotated for gene function using Mercator4
663 (Lohse et al., 2014). Significantly affected gene categories were determined by
664 MapMan using a Wilcoxon rank-sum test with the Benjamini-Hochberg-Yekutieli
665 procedure to correct for the false discovery rate. All MapMan annotations and statistical
666 analyses are available for review in supplemental data. The lists of differentially
667 expressed genes from AZD-8055-treated and MTX-treated samples were compared
668 using a hypergeometric test for significant overlap using R software (phyper function).
669 For comparative analysis, only those genes that could be detected in both the MTX and
670 AZD-8055 treatment transcriptomes (i.e., the ~22,000 genes with complementary
671 probes in the CATMA microarray) were considered.

672 **Seedling chemical treatment assays**

673 *$35S_{PRO}$:S6K1-HA* Col-0 seeds (Xiong and Sheen, 2012) were sterilized with a
674 50% bleach and 0.1% tween-20 solution and stratified in the dark at 4ºC for 2 days in
675 ddH_2O. Each well of a standard 6-well culture plate was filled with 1 mL of ½ MS, pH
676 5.7liquid media. ~20 *$35S_{PRO}$:S6K1-HA* Col-0 seeds were placed in each well under

677 aseptic conditions, and the plate was sealed with micropore tape. Plates were grown at
678 23ºC with a light intensity of 70 μmol m^{-2} s^{-1} photosynthetically active radiation and a 12
679 h day / 12 h night cycle for 3 days. The media were then replaced with ½ MS
680 supplemented with 15 mM D-glucose, pH 5.7, and any other treatments as described in
681 the text, and returned to growth chambers. All treatments, transfers, and seedling
682 collections were performed at subjective dawn unless otherwise noted for consistency.
683 Photographed seedlings were left in treatment media for 7 days to observe
684 developmental differences.

685 Methotrexate (Gainger), 6-mercaptopurine (Fisher Scientific), 5-fluorouracil
686 (Fisher Scientific), 5-fluoroorotic acid (Fisher Scientific), adenosine-5′-monophosphate
687 disodium (Fisher Scientific), cytidine-5′-monophosphate disodium (Chem-Impex),
688 guanosine-5′-monophosphate disodium (Chem-Impex), inosine-5’-monophosphate
689 (TGI), and uracil 5′-monophosphate trisodium (Chem-Impex) were prepared fresh in
690 concentrated stock solutions that were then diluted in ½ MS media (Caisson Labs), pH
691 = 5.7 with KOH, for application to seedlings.

692

693 **Acknowledgments**

694 This project was supported by NIH DP5-OD-023072 to J.O.B. M.B. is supported by an
695 NSF Graduate Research Fellowship. This work used the Vincent J. Coates Genomics
696 Sequencing Laboratory at UC Berkeley, supported by the NIH-S10-OD018174
697 Instrumentation Grant. We thank De Wood and Tina Williams at USDA ARS for
698 microscopy support, Prof. Jen Sheen for sharing *35S$_{PRO}$:S6K-HA A. thaliana* seeds,
699 Anjuli Matharu for experimental assistance, and Sam Leiboff for assistance with RNA-
700 Seq analysis.

701

702 **Author Contributions**

703 M.B., M.R.S., R.H., and J.O.B. designed the research, performed experiments, and
704 analyzed data. M.B. and J.O.B. wrote the manuscript.

705

706 **References**

707 **Ahn, C.S., Han, J.-A., Lee, H.-S., Lee, S., and Pai, H.-S.** (2011). The PP2A regulatory
708 subunit Tap46, a component of the TOR signaling pathway, modulates growth and
709 metabolism in plants. Plant Cell.

710 **Aird, K.M. and Zhang, R.** (2015). Nucleotide metabolism, oncogene-induced
711 senescence and cancer. Cancer Lett.

712 **Anders, S., Pyl, P.T., and Huber, W.** (2015). HTSeq--a Python framework to work with
713 high-throughput sequencing data. Bioinformatics **31**: 166–169.

714 **Baulcombe, D.C.** (1999). Fast forward genetics based on virus-induced gene silencing.
715 Curr. Opin. Plant Biol.

716 **Ben-Sahra, I., Howell, J.J., Asara, J.M., and Manning, B.D.** (2013). Stimulation of de
717 novo pyrimidine synthesis by growth signaling through mTOR and S6K1. Science
718 (80-.).

719 **Ben-Sahra, I., Hoxhaj, G., Ricoult, S.J.H., Asara, J.M., and Manning, B.D.** (2016).
720 mTORC1 induces purine synthesis through control of the mitochondrial
721 tetrahydrofolate cycle. Science (80-.).

722 **Bolle, C., Huep, G., Kleinbölting, N., Haberer, G., Mayer, K., Leister, D., and**
723 **Weisshaar, B.** (2013). GABI-DUPLO: A collection of double mutants to overcome
724 genetic redundancy in Arabidopsis thaliana. Plant J.

725 **Brunkard, J.O., Burch-Smith, T.M., Runkel, A.M., and Zambryski, P.C.** (2015).
726 Investigating plasmodesmata genetics with Virus-Induced Gene Silencing and an
727 Agrobacterium-mediated GFP movement assay. In, pp. 185-198 SRC-
728 GoogleScholar FG-0.

729 **Burch-Smith, T.M., Brunkard, J.O., Choi, Y.G., and Zambryski, P.C.** (2011). PNAS
730 Plus: Organelle-nucleus cross-talk regulates plant intercellular communication via
731 plasmodesmata. Proc. Natl. Acad. Sci. **108**: E1451–E1460.

732 **Burch-Smith, T.M. and Zambryski, P.C.** (2010). Loss of increased size exclusion limit

733 (ise)1 or ise2 increases the formation of secondary plasmodesmata. Curr. Biol. **20**:
734 989–993.

735 **Cardenas, M.E., Cutler, N.S., Lorenz, M.C., Di Como, C.J., and Heitman, J.** (1999).
736 The TOR signaling cascade regulates gene expression in response to nutrients.
737 Genes Dev. **13**: 3271–3279.

738 **Chantranupong, L., Wolfson, R.L., and Sabatini, D.M.** (2015). Nutrient-sensing
739 mechanisms across evolution. Cell **161**: 67–83.

740 **Chen, D.L., Delatorre, C.A., Bakker, A., and Abel, S.** (2000). Conditional identification
741 of phosphate-starvation-response mutants in Arabidopsis thaliana. Planta.

742 **Chiou, T.-J. and Lin, S.-I.** (2011). Signaling Network in Sensing Phosphate Availability
743 in Plants. Annu. Rev. Plant Biol.

744 **Cordell, D. and White, S.** (2011). Peak phosphorus: Clarifying the key issues of a
745 vigorous debate about long-term phosphorus security. Sustainability.

746 **Correll, D.L.** (1998). The Role of Phosphorus in the Eutrophication of Receiving
747 Waters: A Review. J. Environ. Qual.

748 **Couso, I. Pérez-Pérez, ME. Ford, MM. Martínez-Force, E. Hicks, LM Umen, JG.**
749 **Crespo, JL. (**2020). Phosphorus Availablity Regulates TORC1 Signaling via LST8
750 in Chlamydomonas. Plant Cell.

751 **Cunningham, J.T., Moreno, M. V., Lodi, A., Ronen, S.M., and Ruggero, D.** (2014).
752 Protein and nucleotide biosynthesis are coupled by a single rate-limiting enzyme,
753 PRPS2, to drive cancer. Cell.

754 **Delarue, M. et al.** (2018). mTORC1 Controls Phase Separation and the Biophysical
755 Properties of the Cytoplasm by Tuning Crowding. Cell.

756 **Dong, P., Xiong, F., Que, Y., Wang, K., Yu, L., Li, Z., and Ren, M.** (2015). Expression
757 profiling and functional analysis reveals that TOR is a key player in regulating
758 photosynthesis and phytohormone signaling pathways in Arabidopsis. Front. Plant
759 Sci. **6**: 677.

760 **Earley, K.W., Haag, J.R., Pontes, O., Opper, K., Juehne, T., Song, K., and Pikaard,**
761 **C.S.** (2006). Gateway-compatible vectors for plant functional genomics and
762 proteomics. Plant J.

763 **Emmanuel, N., Ragunathan, S., Shan, Q., Wang, F., Giannakou, A., Huser, N., Jin,**
764 **G., Myers, J., Abraham, R.T., and Unsal-Kacmaz, K.** (2017). Purine Nucleotide
765 Availability Regulates mTORC1 Activity through the Rheb GTPase. Cell Rep.

766 **Grabiner, B.C., Nardi, V., Birsoy, K., Possemato, R., Shen, K., Sinha, S., Jordan,**
767 **A., Beck, A.H., and Sabatini, D.M.** (2014). A diverse array of cancer-associated
768 MTOR mutations are hyperactivating and can predict rapamycin sensitivity. Cancer
769 Discov.

770 **Hannan, K.M., Brandenburger, Y., Jenkins, A., Sharkey, K., Cavanaugh, A.,**
771 **Rothblum, L., Moss, T., Poortinga, G., McArthur, G.A., Pearson, R.B., and**
772 **Hannan, R.D.** (2003). mTOR-Dependent Regulation of Ribosomal Gene
773 Transcription Requires S6K1 and Is Mediated by Phosphorylation of the Carboxy-
774 Terminal Activation Domain of the Nucleolar Transcription Factor UBF . Mol. Cell.
775 Biol.

776 **Vander Heiden, M.G. and DeBerardinis, R.J.** (2017). Understanding the Intersections
777 between Metabolism and Cancer Biology. Cell.

778 **Hoxhaj, G., Hughes-Hallett, J., Timson, R.C., Ilagan, E., Yuan, M., Asara, J.M., Ben-**
779 **Sahra, I., and Manning, B.D.** (2017). The mTORC1 Signaling Network Senses
780 Changes in Cellular Purine Nucleotide Levels. Cell Rep.

781 **Ito, J., Batth, T.S., Petzold, C.J., Redding-Johanson, A.M., Mukhopadhyay, A.,**
782 **Verboom, R., Meyer, E.H., Millar, A.H., and Heazlewood, J.L.** (2011). Analysis of
783 the Arabidopsis cytosolic proteome highlights subcellular partitioning of central
784 plant metabolism. J. Proteome Res.

785 **Kim, D., Langmead, B., and Salzberg, S.L.** (2015). HISAT: A fast spliced aligner with
786 low memory requirements. Nat. Methods.

787 **Kim, I., Hempel, F.D., Sha, K., Pfluger, J., and Zambryski, P.C.** (2002). Identification

788 of a developmental transition in plasmodesmatal function during embryogenesis in
789 Arabidopsis thaliana. Development **129**: 1261–1272.

790 **Kim, Y.K., Kim, S., Shin, Y.J., Hur, Y.S., Kim, W.Y., Lee, M.S., Cheon, C.I., and**
791 **Verma, D.P.S.** (2014). Ribosomal protein s6, a target of rapamycin, is involved in
792 the regulation of rRNA genes by possible epigenetic changes in arabidopsis. J.
793 Biol. Chem.

794 **Lerbs, S., Wollgiehn, R., and Neumann, D.** (1980). Effect of 5-Fluorouracil on the
795 synthesis of chloroplast and cytoplasmic ribosomal RNA in leaves of Nicotiana
796 rustica. Biochem. und Physiol. der Pflanz. **175**: 516–528.

797 **Liu, Y., Schiff, M., Marathe, R., and Dinesh-Kumar, S.P.** (2002). Tobacco Rar1,
798 EDS1 and NPR1/NIM1 like genes are required for N-mediated resistance to
799 tobacco mosaic virus. Plant J. **30**: 415–429.

800 **Lohse, M., Nagel, A., Herter, T., May, P., Schroda, M., Zrenner, R., Tohge, T.,**
801 **Fernie, A.R., Stitt, M., and Usadel, B.** (2014). Mercator: A fast and simple web
802 server for genome scale functional annotation of plant sequence data. Plant, Cell
803 Environ.

804 **Loizeau, K., De Brouwer, V., Gambonnet, B., Yu, A., Renou, J.-P., Van Der**
805 **Straeten, D., Lambert, W.E., Rebeille, F., and Ravanel, S.** (2008). A Genome-
806 Wide and Metabolic Analysis Determined the Adaptive Response of Arabidopsis
807 Cells to Folate Depletion Induced by Methotrexate. PLANT Physiol.

808 **López-Arredondo, D.L., Leyva-González, M.A., González-Morales, S.I., López-**
809 **Bucio, J., and Herrera-Estrella, L.** (2014). Phosphate Nutrition: Improving Low-
810 Phosphate Tolerance in Crops. Annu. Rev. Plant Biol.

811 **Love, M.I., Huber, W., and Anders, S.** (2014). Moderated estimation of fold change
812 and dispersion for RNA-seq data with DESeq2. Genome Biol.

813 **Marion, R.M., Regev, A., Segal, E., Barash, Y., Koller, D., Friedman, N., and**
814 **O'Shea, E.K.** (2004). Sfp1 is a stress- and nutrient-sensitive regulator of ribosomal
815 protein gene expression. Proc. Natl. Acad. Sci. **101**: 14315–14322.

816 **Meinke, D.W.** (1985). Embryo-lethal mutants of Arabidopsis thaliana: analysis of
817 mutants with a wide range of lethal phases. Theor. Appl. Genet.

818 **Menand, B., Desnos, T., Nussaume, L., Berger, F., Bouchez, D., Meyer, C., and**
819 **Robaglia, C.** (2002). Expression and disruption of the Arabidopsis TOR (target of
820 rapamycin) gene. Proc. Natl. Acad. Sci. U. S. A. **99**: 6422–6427.

821 **Montané, M.H. and Menand, B.** (2013). ATP-competitive mTOR kinase inhibitors delay
822 plant growth by triggering early differentiation of meristematic cells but no
823 developmental patterning change. J. Exp. Bot. **64**: 4361–4374.

824 **Näsholm, T., Ekblad, A., Nordin, A., Giesler, R., Högberg, M., and Högberg, P.**
825 (1998). Boreal forest plants take up organic nitrogen. Nature.

826 **Pelletier, J., Thomas, G., and Volarevi, S.** (2017). Ribosome biogenesis in cancer:
827 New players and therapeutic avenues. Nat. Rev. Cancer.

828 **Ren, M., Qiu, S., Venglat, P., Xiang, D., Feng, L., Selvaraj, G., and Datla, R.** (2011).
829 Target of rapamycin regulates development and ribosomal RNA expression
830 through kinase domain in Arabidopsis. Plant Physiol.

831 **Robitaille, A.M., Christen, S., Shimobayashi, M., Cornu, M., Fava, L.L., Moes, S.,**
832 **Prescianotto-Baschong, C., Sauer, U., Jenoe, P., and Hall, M.N.** (2013).
833 Quantitative phosphoproteomics reveal mTORC1 activates de novo pyrimidine
834 synthesis. Science (80-.).

835 **Saxton, R.A. and Sabatini, D.M.** (2017). mTOR Signaling in Growth, Metabolism, and
836 Disease. Cell.

837 **Schmid, M., Davison, T.S., Henz, S.R., Pape, U.J., Demar, M., Vingron, M.,**
838 **Schölkopf, B., Weigel, D., and Lohmann, J.U.** (2005). A gene expression map of
839 Arabidopsis thaliana development. Nat. Genet. **37**: 501–506.

840 **Shi, L., Wu, Y., and Sheen, J.** (2018). TOR signaling in plants: conservation and
841 innovation. Development.

842 **Springmann, M. et al.** (2018). Options for keeping the food system within

843 environmental limits. Nature.

844 **Stonebloom, S., Burch-Smith, T., Kim, I., Meinke, D., Mindrinos, M., and**
845 **Zambryski, P.** (2009). Loss of the plant DEAD-box protein ISE1 leads to defective
846 mitochondria and increased cell-to-cell transport via plasmodesmata. Proc. Natl.
847 Acad. Sci. U. S. A. **106**: 17229–17234.

848 **Sulpice, R. et al.** (2014). Low levels of ribosomal RNA partly account for the very high
849 photosynthetic phosphorus-use efficiency of Proteaceae species. Plant, Cell
850 Environ.

851 **Theodorou, M.E. and Plaxton, W.C.** (1993). Metabolic Adaptations of Plant
852 Respiration to Nutritional Phosphate Deprivation. Plant Physiol.

853 **Thimm, O., Bläsing, O., Gibon, Y., Nagel, A., Meyer, S., Krüger, P., Selbig, J.,**
854 **Müller, L. a., Rhee, S.Y., and Stitt, M.** (2004). MAPMAN: A user-driven tool to
855 display genomics data sets onto diagrams of metabolic pathways and other
856 biological processes. Plant J. **37**: 914–939.

857 **Valvezan, A.J. et al.** (2017). mTORC1 Couples Nucleotide Synthesis to Nucleotide
858 Demand Resulting in a Targetable Metabolic Vulnerability. Cancer Cell.

859 **Valvezan, A.J. and Manning, B.D.** (2019). Molecular logic of mTORC1 signalling as a
860 metabolic rheostat. Nat. Metab. **1**: 321–333.

861 **Vance, C.P., Uhde-Stone, C., and Allan, D.L.** (2003). Phosphorus acquisition and use:
862 Critical adaptations by plants for securing a nonrenewable resource. New Phytol.

863 **Veneklaas, E.J., Lambers, H., Bragg, J., Finnegan, P.M., Lovelock, C.E., Plaxton,**
864 **W.C., Price, C.A., Scheible, W.R., Shane, M.W., White, P.J., and Raven, J.A.**
865 (2012). Opportunities for improving phosphorus-use efficiency in crop plants. New
866 Phytol.

867 **Witz, S., Jung, B., Fürst, S., and Möhlmann, T.** (2012). De Novo Pyrimidine
868 Nucleotide Synthesis Mainly Occurs outside of Plastids, but a Previously
869 Undiscovered Nucleobase Importer Provides Substrates for the Essential Salvage
870 Pathway in Arabidopsis . Plant Cell.

871 **Wu, Y., Shi, L., Li, L., Fu, L., Liu, Y., Xiong, Y., and Sheen, J.** (2019). Integration of
872 nutrient, energy, light and hormone signalling via TOR in plants. J. Exp. Bot.

873 **Xiong, Y., McCormack, M., Li, L., Hall, Q., Xiang, C., and Sheen, J.** (2013a).
874 Glucose-TOR signalling reprograms the transcriptome and activates meristems.
875 Nature **496**: 181–186.

876 **Xiong, Y., McCormack, M., Li, L., Hall, Q., Xiang, C., and Sheen, J.** (2013b).
877 Glucose-TOR signalling reprograms the transcriptome and activates meristems.
878 Nature **496**: 181–186.

879 **Xiong, Y. and Sheen, J.** (2012). Rapamycin and glucose-target of rapamycin (TOR)
880 protein signaling in plants. J. Biol. Chem. **287**: 2836–2842.

881 **Xu, G., Fan, X., and Miller, A.J.** (2012). Plant nitrogen assimilation and use efficiency.
882 Annu. Rev. Plant Biol. **63**: 153–82.

883

884 **Figure Legends**

885 **Figure 1.** Ribosomes are major sinks for organic phosphorus in plant cells. **(A)** As much
886 as 50% of organic phosphorus (P_O) is allocated to ribosomal RNA in plant cells. The
887 remaining P_o is allocated to nucleic acids (transfer RNAs (~2%), messenger RNAs
888 (~1%), and DNA (~7%)), phospholipids (~30%), and phosphoesters (~20%), including
889 phosphorylated proteins and metabolites, e.g., free nucleotide triphosphates. **(B)** Plant
890 genomes encode several phosphoribosyl pyrophosphate (PRPP) synthetases (PRSs)
891 that localize to either the cytosol (left) or organelles (right). In *A. thaliana*, there are five
892 *PRS* genes: *PRS4* encodes the only cytosolic PRS, and *PRS1, PRS2, PRS3,* and
893 *PRS5* encode organelle-targeted PRSs. In the cytosol, PRPP is primarily metabolized
894 via the purine salvage and *de novo* pyrimidine synthesis pathways. Conversely, in the
895 organelles, PRPP is metabolized in the pyrimidine salvage and *de novo* purine
896 synthesis pathways.

897 **Figure 2. Cytosolic PRS (PRS4) drives plant development and TOR activity in *N.***
898 ***benthamiana*. (A)** Silencing *PRS4* drastically reduces TOR activity. S6K-pT449 levels
899 reflect TOR activity, because S6K-T449 is a direct substrate of TOR (Xiong and Sheen,
900 2012). S6K-pT449 and total S6K levels were assayed by Western blots in knockdown
901 TRV::*NbPRS4* plants or mock controls (representative images shown here).
902 Quantification of band densities confirmed that S6K-pT449 levels decrease ~5-fold in
903 TRV::*NbPRS4* knockdowns, but total S6K levels are not affected in TRV::*NbPRS4*. **(B)**
904 *PRS4* is required for shoot development. There are fewer leaves in TRV::*NbPRS4*
905 knockdowns, and the leaves are misshapen and small. We observed individual-to-
906 individual variation in phenotypic severity after silencing *PRS4* by VIGS; a
907 representative of the "moderate" TRV::*NbPRS4* phenotype and of the "severe"
908 TRV::*NbPRS4* phenotype are shown. Outlines of leaf shapes are shown, including all
909 leaves with silenced *PRS4* expression (i.e., only leaves above the primary infected leaf),
910 with the oldest leaf on the left and the youngest leaf on the right. **(C)** Silencing *PRS4*
911 impairs cell expansion and cell division. Epidermal pavement cell shape was not
912 dramatically altered in TRV::*NbPRS4* knockdowns, but epidermal pavement cell size
913 was significantly lower. This difference in cell size is insufficient to account for the
914 decrease in total leaf area shown in panel B; therefore, there are also fewer epidermal
915 pavement cells in TRV::*NbPRS4*. **(D)** We did not observe clear effects of silencing
916 *PRS4* on vegetative shoot apical meristem morphology.

917 **Figure 3. Cytosolic PRS4 is required for embryogenesis. (A)** *PRS4* is encoded by
918 *At2g42910*. We isolated an insertional allele, GK-780B11, that we named *prs4-1*. **(B)**
919 Representative silique of a self-fertilized *prs4-1* / + heterozygous parent. 23% of seeds
920 are *prs4-1 / prs4-1* homozygotes; these seeds are shrunken and brown. **(C)**
921 Homozygous *prs4-1* seeds have no readily visible embryo after clearing. A sibling WT
922 seed from the same silique with a clearly visible early torpedo-shaped embryo is shown
923 for comparison. **(D)** *$35S_{PRO}$:YFP-PRS4* expressed in *A. thaliana* localizes to the
924 cytoplasm.

925 **Figure 4. Silencing *PRS4* reprograms the transcriptome to repress ribosome**
926 **biogenesis. (A)** Scatterplots of gene expression changes in *N. benthamiana* after
927 VIGS. 4,986 genes were significantly differentially expressed between TRV::*NbPRS4*
928 knockdowns with severe phenotypes and mock plants (top panel), but only 489 genes
929 were significantly differentially expressed between TRV::*NbPRS4* knockdowns with
930 severe versus moderate phenotypes (middle panel). Principal component analysis
931 demonstrates that the mock-treated transcriptomes are readily distinguished from the
932 TRV::*NbPRS4* knockdowns, but that the TRV::*NbPRS4* transcriptomes from plants with
933 severe or moderate phenotypes are not grouped separately. **(B)** MapMan functional
934 analysis of DEGs in TRV::*NbPRS4* revealed 48 significantly-affected categories ($p_{adj.}$ <
935 0.05). Categories with primarily repressed gene expression are indicated in blue;
936 categories with primarily induced gene expression are indicated in magenta; categories
937 with genes that are both induced and repressed (e.g., transcription factors) are shown in
938 grey. **(C)** Transcription factor mRNA levels are significantly different in TRV::*NbPRS4*
939 knockdowns. Select transcription factor families typically involved in plant development
940 (C2C2, Cys_2Cys_2 Zn-finger family; MADS, MCM1/AGAMOUS/DEFICIENS/SRF box
941 family; GRF, GROWTH-REGULATING FACTOR family; LOB, LATERAL ORGAN
942 BOUNDARIES family; and the homeobox family) or plant stress responses (ERF,
943 ETHYLENE RESPONSE FACTOR family, excluding AP2 orthologues; bZIP, basic
944 Leucine Zipper Domain family; HSF, Heat Shock Factor; NAC, NAM/ATAF1/CUC2
945 family; and the WRKY family). **(D)** mRNAs encoding 51 subunits of the plant cytosolic
946 ribosome were down-regulated in TRV::*NbPRS4* (shown in this model of a ribosome in
947 blue); mRNAs encoding 2 subunits were up-regulated (magenta). There was ~50% less
948 total rRNA in TRV::*NbPRS4* knockdowns (*p < 0.05). **(E)** Transcriptomic analysis
949 demonstrates that PRS4 is required to promote expression of genes that contribute to
950 ribosome biogenesis (purple, right) and cell cycle progression, and to repress induction
951 of starvation and oxidative stress response genes, including solute transporters and
952 antioxidant glutathione S-transferases (rainbow, left).

953 **Figure 5. Silencing key genes in nucleotide biosynthesis inhibits TOR activity. (A)**
954 Nucleotide biosynthesis is necessary for normal shoot development and physiology.
955 Silencing genes downstream of *PRS4* in nucleotide biosynthesis in *N. benthamiana*
956 reduced leaf number and size, disrupted leaf shape, and caused chlorosis, similar to the
957 phenotypes observed in TRV::*NbPRS4* plants. Each gene was silenced in at least six
958 plants per experiment, and the entire experiment was replicated three times;
959 representative individuals of each silenced gene are shown. **(B)** Silencing nucleotide
960 biosynthesis genes lowers TOR activity. S6K-pT449 levels are strongly reduced in
961 silenced plants compared to mock-infected controls, and the S6K-pT449/S6K ratios are
962 consistently lower.

963 **Figure 6. Chemically inhibiting nucleotide biosynthesis suppresses TOR activity.**
964 **(A)** PRPP synthesized by cytosolic PRS4 is primarily used for purine salvage and *de*
965 *novo* pyrimidine synthesis. 6MP specifically inhibits purine salvage, 5FOA and 5FU
966 specifically inhibit *de novo* pyrimidine synthesis, and MTX broadly inhibits nucleotide
967 biosynthesis. **(B)** Seedlings were grown to quiescence, and then treated with either 15

968 mM glucose, which activates TOR and promotes root elongation (Xiong et al., 2013a),
969 or 15 mM glucose and 10 μM MTX, 6MP, 5FU, or 5FOA, which limit nucleotide
970 biosynthesis. Seedling growth was most drastically impaired in the presence of MTX,
971 which inhibits all nucleotide biosynthesis. Treatment with 5FOA strongly impacted
972 seedling growth as well, while 5FU and 6MP had less dramatic effects **(C)** Seedlings
973 were treated with 10 μM of each inhibitor shown in panel A for 24 h. TOR activity was
974 assayed using Western blots against S6K-pT449 and total S6K, with Ponceau staining
975 shown as a loading control. MTX, 5FU, and 5FOA all reduced TOR activity. 6MP had
976 no reproducible effect. This experiment was repeated three times; representative
977 results are shown here. **(D)** Seedlings were grown as described in panel 6B and
978 treated with either 0.1 μM, 1 μM, 5 μM, 10 μM, or 20 μM MTX. A photograph was taken
979 7 days after treatment. Growth was inhibited by all concentrations of MTX tested. **(E)**
980 TOR activity was assayed using Western blots against S6K-pT449 and total S6K, with
981 Ponceau staining shown as a loading control. 24-hour MTX treatment is effective at
982 inhibiting TOR activity at a concentration as low as 0.1 μM, and1.0 μM MTX treatment
983 effectively inactivates TOR entirely. **(F)** Seedlings were grown as described in panel 6B
984 and treated with either 0.1 μM, 1 μM, 5 μM, 10 μM, or 20 μM 5FOA. A photograph was
985 taken 7 days after treatment. 1 μM 5FOA was sufficient to noticeably delay seedling
986 growth, and higher concentrations had more strong effects on inhibiting development.
987 **(G)** TOR activity was assayed using Western blots against S6K-pT449 and total S6K,
988 with Ponceau staining shown as a loading control. A 24-hour treatment with 5FOA has
989 some effect at 0.1 μM, and strongly lowers TOR activity at concentrations ≥ 1.0 μM.

990 **Figure 7. Nucleotide supply rescues TOR activity in MTX-treated seedlings. (A)**
991 Seedlings were treated with 0.1 μM MTX and collected over a time course, as indicated.
992 TOR activity decrease 3 h after MTX treatment. This experiment was repeated three
993 times; representative results are shown here. **(B,C,D)** Seedlings were pre-treated with
994 0.1 μM MTX for 3.5 h, and then supplied either inosine 5'-monophosphate (IMP) **(B)**,
995 uracil 5'-monophosphate (UMP) **(C)**, or a mixture of nucleotide monophosphates
996 (NMPs) **(D)** at physiologically-relevant concentrations (0.5, 1.0, or 2.0 mM). NMPs
997 restored S6K-pT449 levels and S6K-pT449/S6K ratios in MTX-treated seedlings,
998 suggesting that the effects of MTX on TOR activity are due to nucleotide depletion.
999 Neither IMP nor UMP was sufficient to restore TOR activity, indicating that all
1000 nucleotides (purines and pyrimidines) are required to stimulate TOR in MTX-treated
1001 seedlings. This experiment was repeated five times; representative results are shown
1002 here.

1003 **Figure 8. TOR coordinates nucleotide metabolism with ribosome biogenesis in**
1004 **plants. (A,B)** Enzymes for each step of *de novo* pyrimidine (left) and *de novo* purine
1005 (right) biosynthetic pathways are shown. Fold-change in mRNA levels of these
1006 enzymes in (**A**) the glucose-TOR transcriptome (Xiong et al., 2013a) or (**B**) TOR-
1007 inhibited AZD8055 transcriptome (Dong et al., 2015) are indicated by color, as in panel
1008 C (induced genes are shown in magenta, repressed genes are shown in blue, grey
1009 indicates no detected difference in mRNA levels). **(C)** The set of significant DEGs after
1010 24 h treatment with TOR inhibitor AZD8055 or nucleotide biosynthesis inhibitor MTX
1011 significantly overlap ($p < 10^{-69}$), and 91% of overlapping DEGs are co-regulated. For
1012 details, see Supplemental Data Set 6. **(D)** Metabolites activate TOR to drive ribosome

1013 biogenesis. TOR integrates multiple metabolic signaling pathways in plants by sensing
1014 glucose, nucleotide, and (speculatively) amino acid levels. When other nutrients are
1015 available (e.g., upon glucose activation of TOR), TOR also drives nucleotide
1016 biosynthesis, which both reinforces TOR activity and metabolically supports rRNA
1017 synthesis to contribute to ribosome biogenesis.

1018 **Supplemental Figure 1. *PRS4* is expressed throughout plant development.** *PRS4*
1019 expression shown in the *A. thaliana* eFP browser (top panel); magenta indicates high
1020 relative transcript abundance, white indicates low relative transcript abundance. *PRS4*
1021 is most strongly expressed in metabolically active developmental stages, such as
1022 imbibed (germinating) seeds and shoot apices. Expression patterns of all *PRS* genes,
1023 except for *PRS1*, are shown in a bar graph (bottom panel). *PRS4* is consistently
1024 expressed at higher levels that the other *PRS* genes, except for during late seed
1025 development and in mature pollen.

1026 **Supplemental Figure 2. (A)** RNA was extracted from shoot apices of *N. benthamiana*
1027 plants as shown. **(B)** Schematic of seedling treatment assays. Briefly, after
1028 stratification, seeds were germinated at subjective dawn in ½ MS and allowed to grow
1029 for three days (to quiescence). Seedling media was then replaced with ½ MS and 15
1030 mM D-glucose, and left for 24 h to activate TOR and initiate growth. Then, seedlings
1031 were treated with 0.1 μM MTX or other nucleotide biosynthesis inhibitors, and collected
1032 as described in the text. Alternatively, after 24 h treatment with MTX, plants were re-
1033 supplied with nucleotide monophosphates,, or mock treatments, and collected for
1034 analysis.

1035

1036 **Supplemental Data Set 1.** Significant DEGs in TRV::*NbPRS4* knockdown *N.*
1037 *benthamiana*.

1038 **Supplemental Data Set 2.** Complete transcriptome of TRV::*NbPRS4* knockdown *N.*
1039 *benthamiana*.

1040 **Supplemental Data Set 3.** Significant DEGs in moderate versus severe TRV::*NbPRS4*
1041 knockdown *N. benthamiana*.

1042 **Supplemental Data Set 4.** Mercator4 annotation of the Nb-1 v1.0.1 transcriptome.

1043 **Supplemental Data Set 5.** MapMan functional analysis of the TRV::*NbPRS4*
1044 transcriptome.

1045 **Supplemental Data Set 6.** Transcriptomes of *A. thaliana* treated with MTX, AZD8055,
1046 or glucose-TOR treatments.

1047 **Supplemental Data Set 7.** MapMan functional analysis of the MTX transcriptome.

1048 **Supplemental Data Set 8.** Oligonucleotides used in this study.

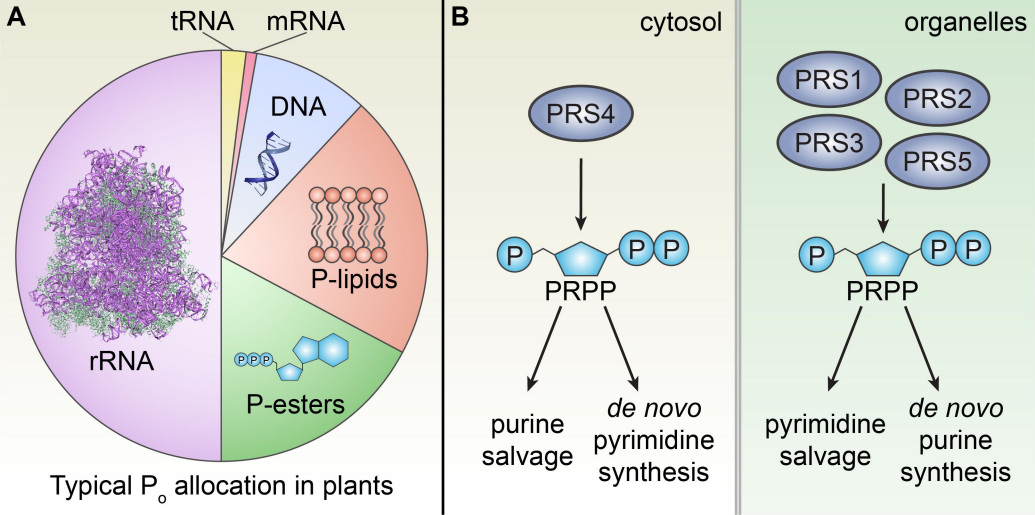
A
tRNA
mRNA
DNA
P-lipids
rRNA
PPP
P-esters
Typical P_o allocation in plants
B
cytosol
PRS4
P
P
P
PRPP
purine salvage
de novo pyrimidine synthesis
organelles
PRS1
PRS2
PRS3
PRS5
P
P
P
PRPP
pyrimidine salvage
de novo purine synthesis

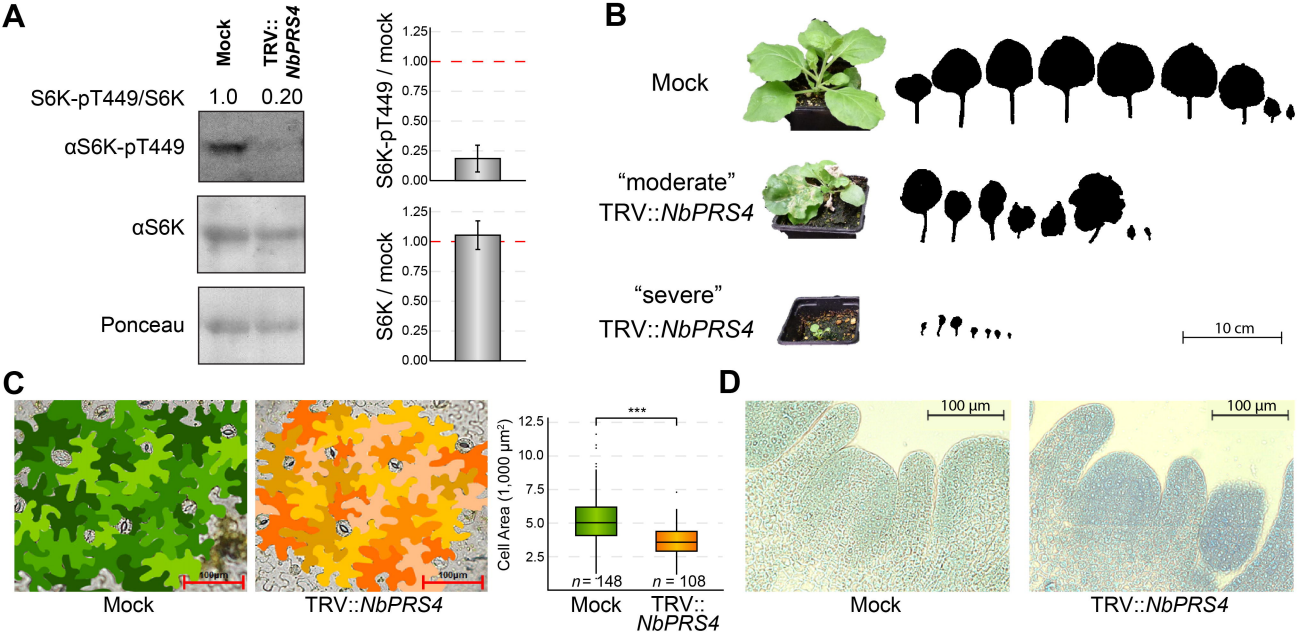
A
Mock
TRV::NbPRS4
S6K-pT449/S6K
1.0
0.20
αS6K-pT449
αS6K
Ponceau
S6K-pT449 / mock
S6K / mock
1.25
1.00
0.75
0.50
0.25
0.00
B
Mock
"moderate" TRV::NbPRS4
"severe" TRV::NbPRS4
10 cm
C
100µm
Mock
TRV::NbPRS4
Cell Area (1,000 µm²)
12.5
10.0
7.5
5.0
2.5
***
n = 148
n = 108
Mock
TRV::NbPRS4
D
100 µm
Mock
TRV::NbPRS4

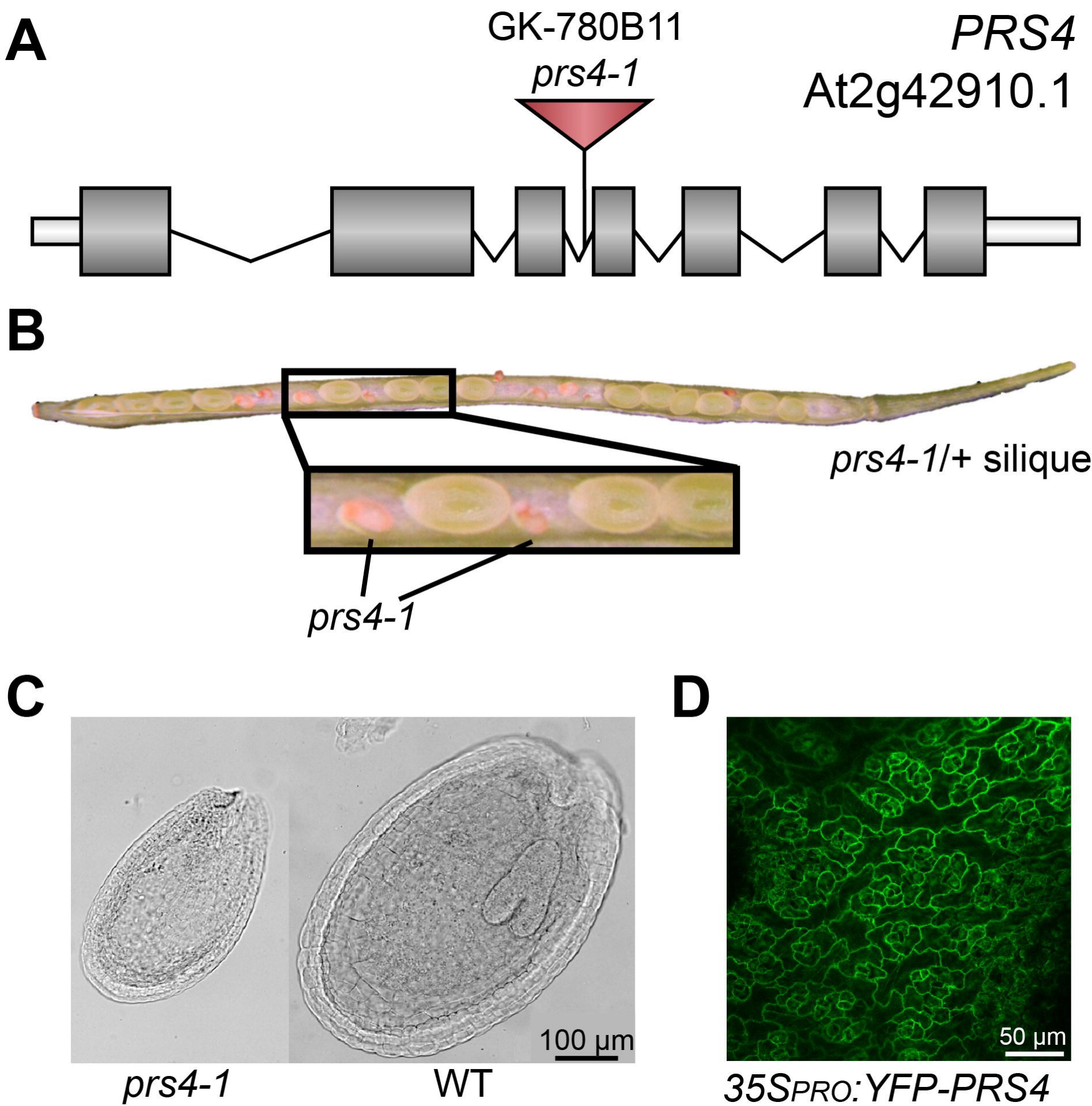
A
GK-780B11
prs4-1
PRS4
At2g42910.1
B
prs4-1/+ silique
prs4-1
C
100 µm
prs4-1
WT
D
50 µm
35SPRO:YFP-PRS4

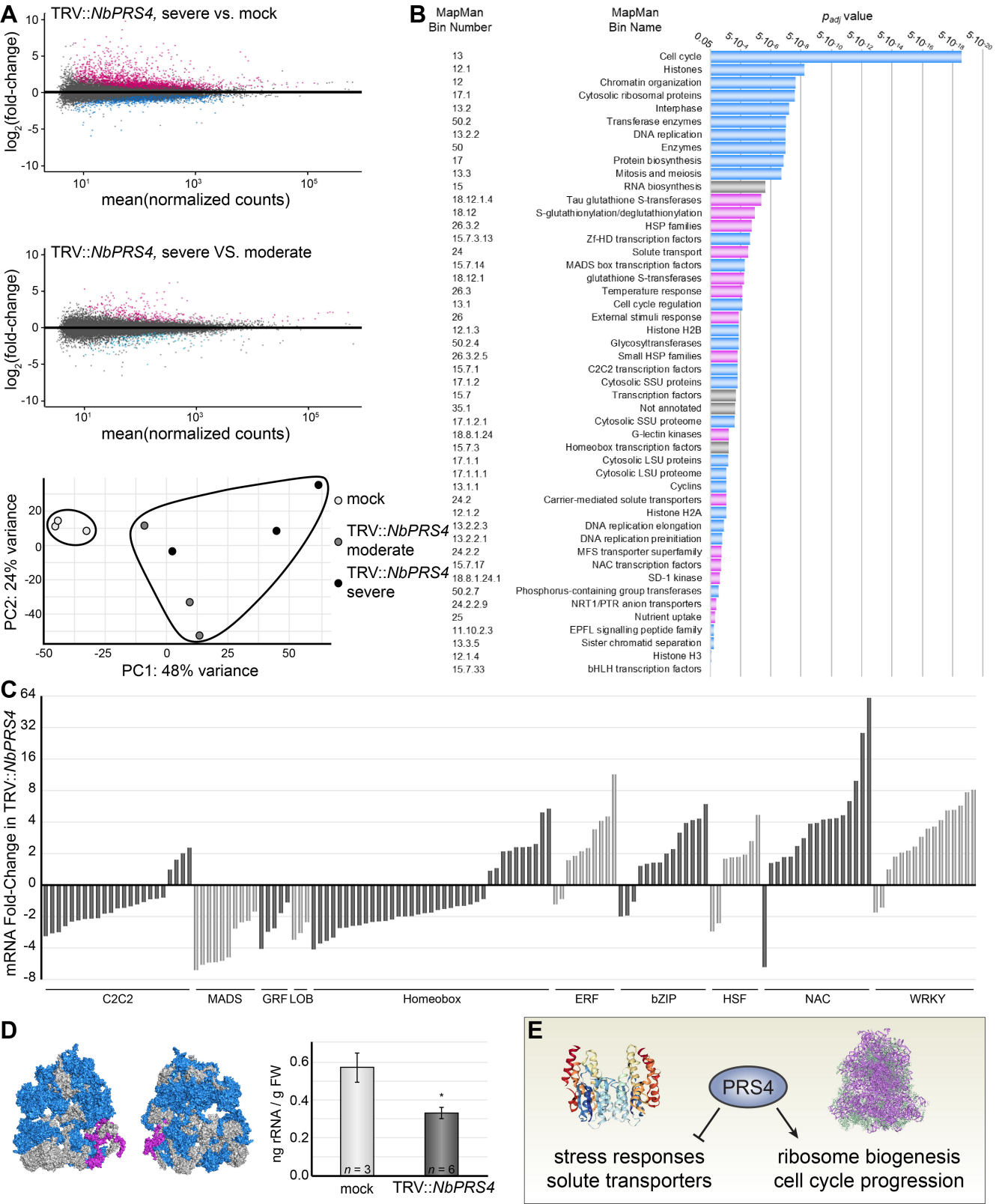
A
TRV::NbPRS4, severe vs. mock
log2(fold-change)
mean(normalized counts)
TRV::NbPRS4, severe VS. moderate
log2(fold-change)
mean(normalized counts)
PC2: 24% variance
PC1: 48% variance
mock
TRV::NbPRS4 moderate
TRV::NbPRS4 severe
B
MapMan Bin Number
MapMan Bin Name
padj value
Cell cycle
Histones
Chromatin organization
Cytosolic ribosomal proteins
Interphase
Transferase enzymes
DNA replication
Enzymes
Protein biosynthesis
Mitosis and meiosis
RNA biosynthesis
Tau glutathione S-transferases
S-glutathionylation/deglutathionylation
HSP families
Zf-HD transcription factors
Solute transport
MADS box transcription factors
glutathione S-transferases
Temperature response
Cell cycle regulation
External stimuli response
Histone H2B
Glycosyltransferases
Small HSP families
C2C2 transcription factors
Cytosolic SSU proteins
Transcription factors
Not annotated
Cytosolic SSU proteome
G-lectin kinases
Homeobox transcription factors
Cytosolic LSU proteins
Cytosolic LSU proteome
Cyclins
Carrier-mediated solute transporters
Histone H2A
DNA replication elongation
DNA replication preinitiation
MFS transporter superfamily
NAC transcription factors
SD-1 kinase
Phosphorus-containing group transferases
NRT1/PTR anion transporters
Nutrient uptake
EPFL signalling peptide family
Sister chromatid separation
Histone H3
bHLH transcription factors
C
mRNA Fold-Change in TRV::NbPRS4
C2C2
MADS
GRF
LOB
Homeobox
ERF
bZIP
HSF
NAC
WRKY
D
ng rRNA / g FW
n = 3
n = 6
mock
TRV::NbPRS4
E
PRS4
stress responses
solute transporters
ribosome biogenesis
cell cycle progression

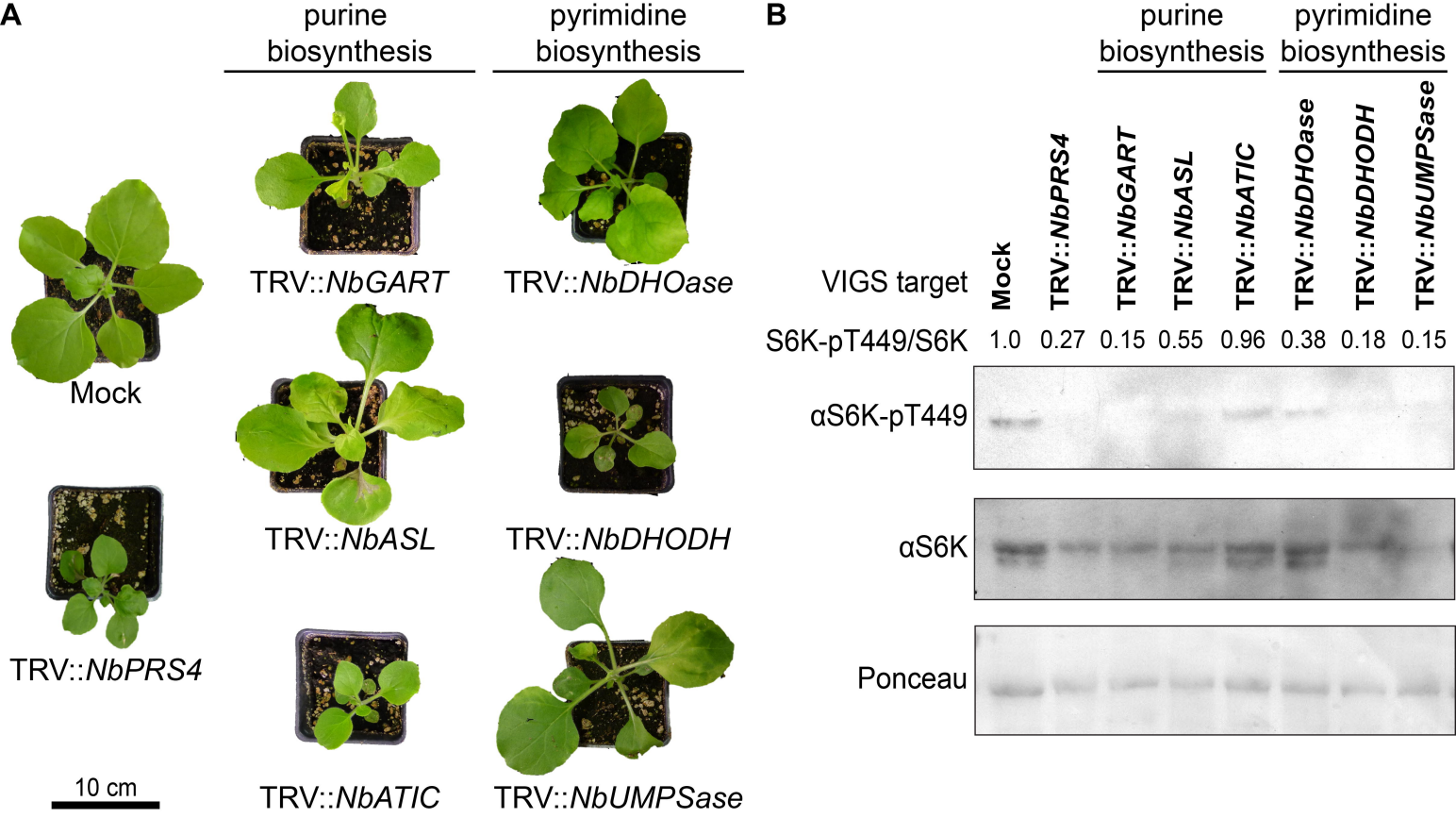
A
purine biosynthesis
pyrimidine biosynthesis
Mock
TRV::NbGART
TRV::NbDHOase
TRV::NbASL
TRV::NbDHODH
TRV::NbPRS4
TRV::NbATIC
TRV::NbUMPSase
10 cm
B
purine biosynthesis
pyrimidine biosynthesis
VIGS target
Mock
TRV::NbPRS4
TRV::NbGART
TRV::NbASL
TRV::NbATIC
TRV::NbDHOase
TRV::NbDHODH
TRV::NbUMPSase
S6K-pT449/S6K
1.0
0.27
0.15
0.55
0.96
0.38
0.18
0.15
αS6K-pT449
αS6K
Ponceau

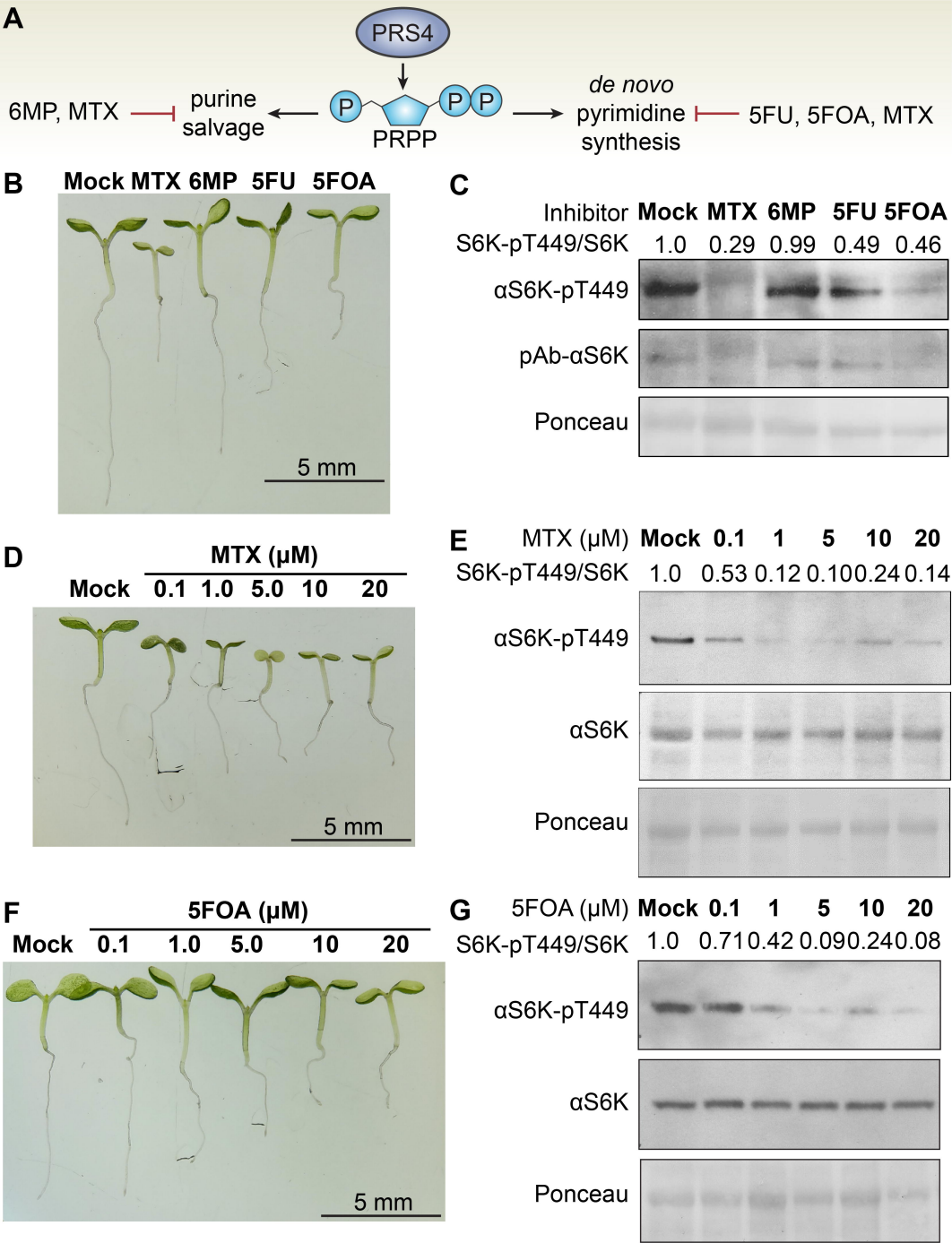
A
PRS4
6MP, MTX
purine salvage
P
P
P
PRPP
de novo pyrimidine synthesis
5FU, 5FOA, MTX
B
Mock MTX 6MP 5FU 5FOA
5 mm
C
Inhibitor Mock MTX 6MP 5FU 5FOA
S6K-pT449/S6K 1.0 0.29 0.99 0.49 0.46
αS6K-pT449
pAb-αS6K
Ponceau
D
MTX (μM)
Mock 0.1 1.0 5.0 10 20
5 mm
E
MTX (μM) Mock 0.1 1 5 10 20
S6K-pT449/S6K 1.0 0.53 0.12 0.10 0.24 0.14
αS6K-pT449
αS6K
Ponceau
F
5FOA (μM)
Mock 0.1 1.0 5.0 10 20
5 mm
G
5FOA (μM) Mock 0.1 1 5 10 20
S6K-pT449/S6K 1.0 0.71 0.42 0.09 0.24 0.08
αS6K-pT449
αS6K
Ponceau

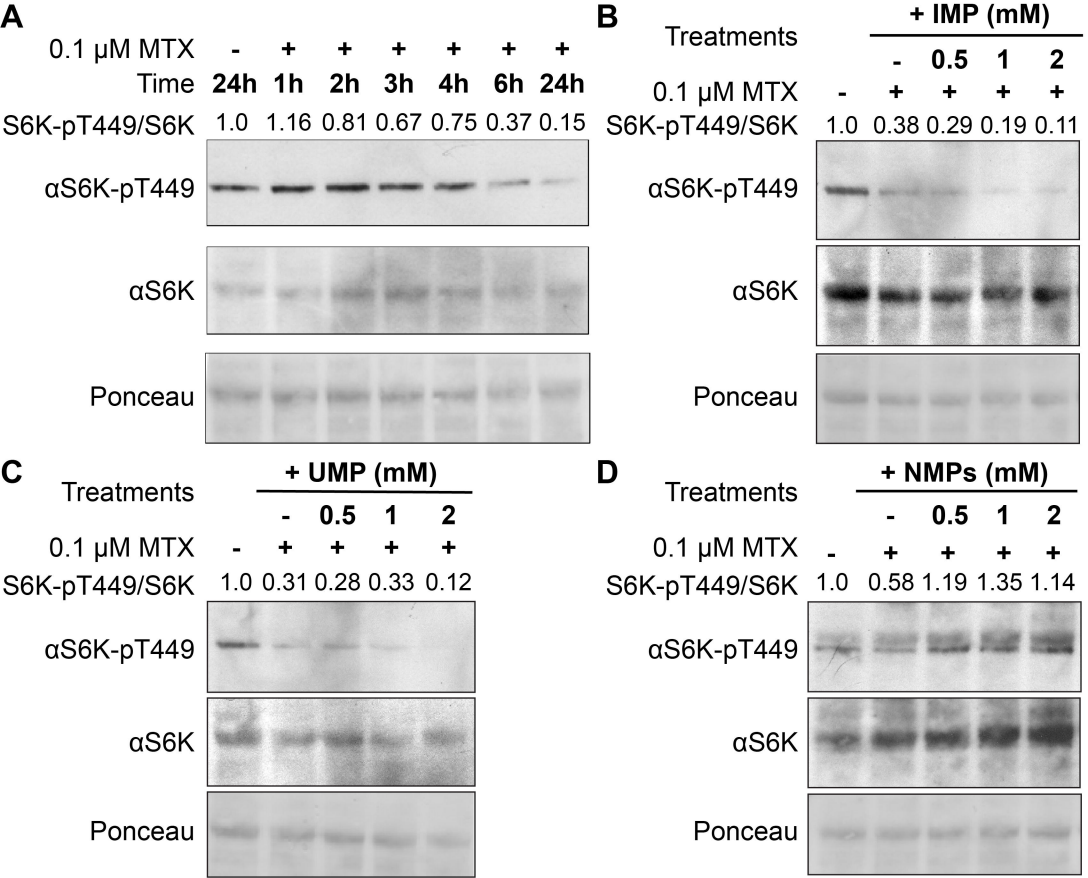
A
0.1 μM MTX - + + + + + +
Time 24h 1h 2h 3h 4h 6h 24h
S6K-pT449/S6K 1.0 1.16 0.81 0.67 0.75 0.37 0.15
αS6K-pT449
αS6K
Ponceau
B
Treatments
+ IMP (mM)
- 0.5 1 2
0.1 μM MTX - + + + +
S6K-pT449/S6K 1.0 0.38 0.29 0.19 0.11
αS6K-pT449
αS6K
Ponceau
C
Treatments
+ UMP (mM)
- 0.5 1 2
0.1 μM MTX - + + + +
S6K-pT449/S6K 1.0 0.31 0.28 0.33 0.12
αS6K-pT449
αS6K
Ponceau
D
Treatments
+ NMPs (mM)
- 0.5 1 2
0.1 μM MTX - + + + +
S6K-pT449/S6K 1.0 0.58 1.19 1.35 1.14
αS6K-pT449
αS6K
Ponceau

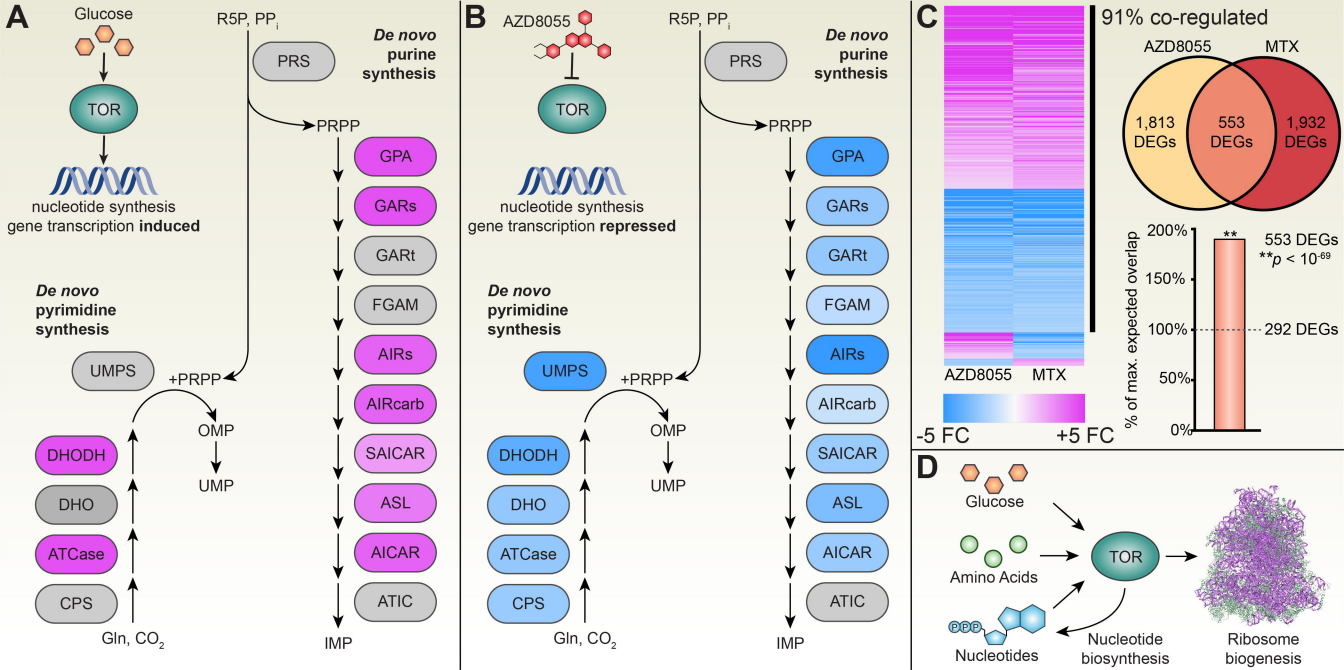
A
Glucose
TOR
nucleotide synthesis
gene transcription induced
R5P, PPi
PRS
De novo purine synthesis
PRPP
GPA
GARs
GARt
FGAM
AIRs
AIRcarb
SAICAR
ASL
AICAR
ATIC
IMP
De novo pyrimidine synthesis
UMPS
+PRPP
OMP
UMP
DHODH
DHO
ATCase
CPS
Gln, CO2
B
AZD8055
TOR
nucleotide synthesis
gene transcription repressed
R5P, PPi
PRS
De novo purine synthesis
PRPP
GPA
GARs
GARt
FGAM
AIRs
AIRcarb
SAICAR
ASL
AICAR
ATIC
IMP
De novo pyrimidine synthesis
UMPS
+PRPP
OMP
UMP
DHODH
DHO
ATCase
CPS
Gln, CO2
C
91% co-regulated
AZD8055
MTX
1,813 DEGs
553 DEGs
1,932 DEGs
AZD8055
MTX
-5 FC
+5 FC
% of max. expected overlap
200%
150%
100%
50%
0%
**
553 DEGs
**p < 10-69
292 DEGs
D
Glucose
Amino Acids
TOR
Nucleotides
Nucleotide biosynthesis
Ribosome biogenesis